UCLA
COMPUTATIONAL AND APPLIED MATHEMATICS

The Geometry of Wulff Crystal Shapes and Its Relations with Riemann Problems

Danping Peng
Stanley Osher
Barry Merriman
Hong-Kai Zhao

December 1998

CAM Report 98-51

Department of Mathematics
University of California, Los Angeles
Los Angeles, CA. 90095-1555

http://www.math.ucla.edu/applied/cam/index.html

The Geometry of Wulff Crystal Shapes and Its Relations with Riemann Problems

Danping Peng, Stanley Osher, Barry Merriman, and Hong-Kai Zhao

ABSTRACT. In this paper we begin to explore the mathematical connection between equilibrium shapes of crystalline materials (Wulff shapes) and shock wave structures in compressible gas dynamics (Riemann problems). These are radically different physical phenomena, but the similar nature of their discontinuous solutions suggests a connection.

We show there is a precise sense in which any two dimensional crystalline form can be described in terms of rarefactions and contact discontinuities for an associated scalar hyperbolic conservation law. As a byproduct of this connection, we obtain a new analytical formula for crystal shapes in two dimension. We explore a possible extension to high dimensions.

We also formulate the problem in the level set framework and present a simple algorithm using the level set method to plot the approximate equilibrium crystal shape corresponding to a given surface energy function in two and three dimensions.

Our main motivation for establishing this connection is to encourage a transfer of theoretical and numerical techniques between the rich but disparate disciplines of crystal growth and gas dynamics. The work reported here represents a first step towards this goal.

CONTENTS

Research supported by DARPA/NSF VIP grant:NSF grant DMS9615854 and NSF grant DMS9706827.

1. Introduction

In this paper we develop a mathematical connection between two quite different physical phenomena: the shapes of crystalline materials, and dynamics of shock waves in a gas.

Both of these phenomena have long research histories: The problem of determining the equilibrium shape of a perfect crystal was posed and first solved by Wulff in 1901 [**28**]. In nature this ideal "Wulff shape" (see figure 1) is observed in crystals that are small enough to relax to their lowest energy state without becoming stuck in local minima.

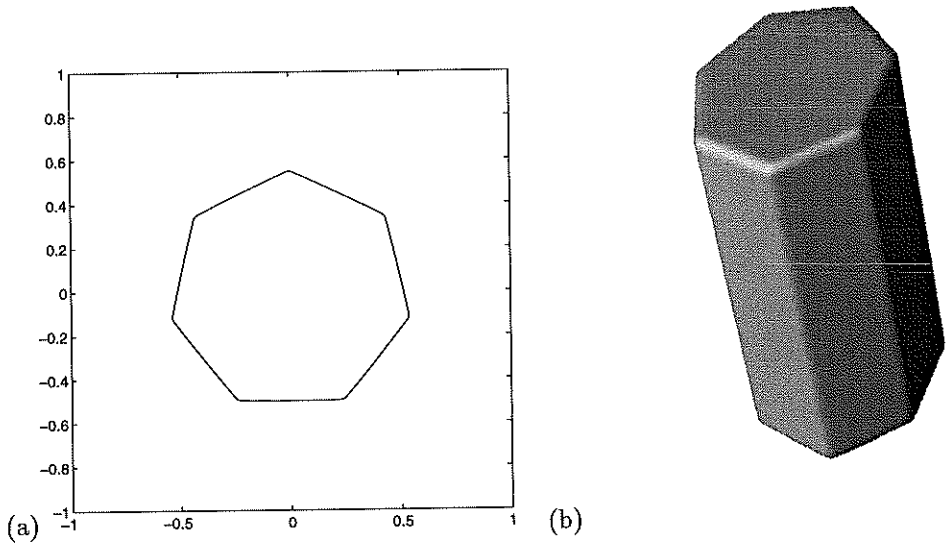

FIGURE 1. *(a) A 2D Wulff crystal. (b) A 3D Wulff crystal.*

The problem of determining the dynamics of a gas initialized with an arbitrary initial jump in state was posed and partially solved by Riemann in 1860 [**21**]. Solutions to this "Riemann problem" can be observed experimentally in shock tubes, where a membrane separating gases in different uniform states is rapidly removed. The Riemann problem has since been generalized to mean the solution of any system of hyperbolic conservation laws subject to initial data prepared with a single jump in state separating two regions with different constant states.

The intuitive link between Wulff crystals and Riemann problems is the similar nature of the discontinuous solutions. Crystalline shapes are characterized by perfectly flat faces—facets—separated by sharp edges, whereas shocked gases are characterized by regions of constant pressure separated by steep jumps (see figure 2). It is tempting to imagine that the sharp edges in a crystal shape can be though of as shock waves in some sense.

To explore this shock wave-crystal edge analogy more precisely, we represent the crystal surface in terms of its unit normal vector. The normal has regions of constant direction separated by jumps in direction, which suggests it may satisfy the same sort of equations—hyperbolic conservation laws—that govern shocks in nonlinear gas dynamics. The analogy continues to hold if we consider the most general behaviors of Wulff crystals and Riemann problems: Wulff shapes are constructed entirely from facets, rounded faces and sharp edges, for which the normal direction has regions of constancy, smooth variation, and isolated jumps. Correspondingly, the solution to a Riemann problem for any hyperbolic conservation law is constructed entirely from constant states, rarefactions (smooth variation), and shocks or contacts (isolated jumps).

We will show that the precise connection is this: the normal vector to the Wulff shape of a crystal in *two dimensions* is the time self-similar solution of an associated Riemann problem for a hyperbolic conservation law. In this representation, it does indeed turn out that crystal facets are the constant states in the Riemann problem and the curved faces are the rarefactions, but the sharp corners are contact discontinuities, not shocks.

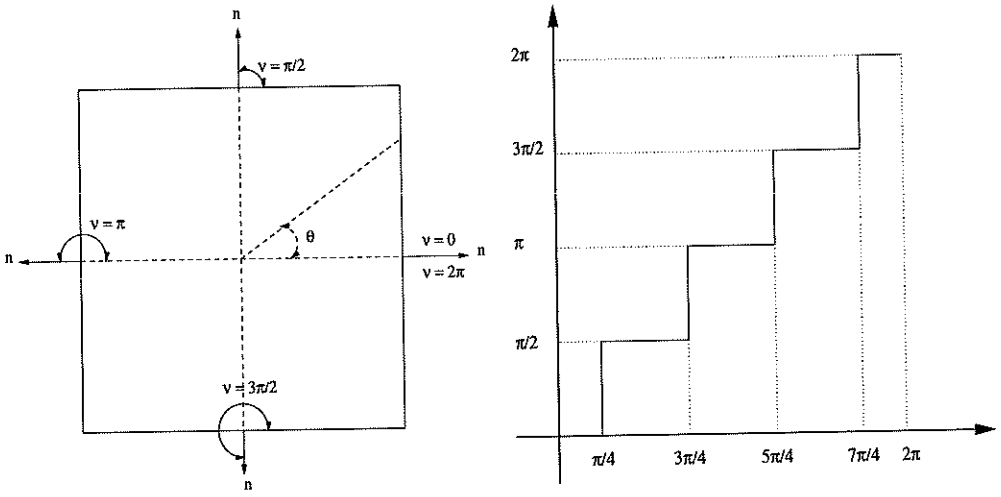

FIGURE 2. *The left is a 2D square Wulff crystal. The right is the plot of the angle between outward normal and the horizontal axis vs the polar angle.*

The most immediate consequences of this representation is a new analytical formula for the Wulff shape, derived using formulas and methods from the theory of Riemann problems.

For clarity, we will summarize the analytical results here; these are explained in detail as they are derived in the main text. Let the Wulff shape be described in a polar coordinate system with the origin at its center. Choose the horizontal axis such that it intersects with the Wulff shape at a point where the unit normal to the Wulff shape coincides with the horizontal axis. (For example, the horizontal axis can be chosen as the line emanating from the origin and passing through the minima of the surface tension.) The boundary curve of the shape can be parameterized by giving the angle ν between the normal and the horizontal axis as a function of the polar angle θ. This curve $\nu(\theta)$ gives the time self-similar viscosity solution $\nu(\xi,t) = \nu(\xi/t)$ to the hyperbolic conservation law

$$\nu_t + F(\nu)_\xi = 0 \tag{1.1}$$

with flux function

$$F(\nu) = \frac{1}{2}\nu^2 + \int_0^\nu \tan^{-1}\left(\frac{\hat{\gamma}'(u)}{\hat{\gamma}(u)}\right) du \tag{1.2}$$

and initial data

$$\nu(\xi < 0, t = 0) = 0, \tag{1.3}$$

$$\nu(\xi > 0, t = 0) = 2\pi, \tag{1.4}$$

where $\gamma(\nu)$ is the crystalline surface tension as a function of the surface normal direction, $\hat{\gamma}(\nu)$ is the Frank convexification of $\gamma(\nu)$ (described in section 3.4) and $\tan^{-1}$ has range $[-\pi/2, \pi/2]$. The new formula for the Wulff shape that results from this connection is

$$\nu(\theta) = -\frac{d}{d\theta} \min_{0 \le \nu \le 2\pi} [F(\nu) - \theta\nu], \tag{1.5}$$

where F is the flux function from the conservation law.

The primary goal of this paper is to expose the connection between faceted crystal shapes and shock waves and related phenomena from gas dynamics. Because readers familiar with the theory of Wulff shapes come from a material science background, they are unlikely to know the theory of Riemann problems from the field of gas dynamics, and vice versa. To fill in these likely gaps, we will present the elementary background for both problems prior to deriving our new results. Most of our proof will be somewhat formal, referring the mathematically inclined readers to relevant publications for rigorous treatment. In addition to making the present paper more readable, we hope this inclusive approach will foster future interaction between these two disparate research communities.

The paper is organized as follows: we start with the essential background on the Wulff problem and the Riemann problem, emphasizing their similarities. Then we show how to represent the Wulff shape as the solution to a Riemann problem, via two seemingly quite different approaches: the first approach starts from the Euler-Lagrange equation of the surface energy and connects it with the Riemann problem of a scalar conservation law under a suitable choice of variables. The other approach uses the self-similar growth property of the Wulff shape and shows that it solves a Riemann problem for the same conservation law. In the process, we develop the new formula (1.5). We present two simple illustrative examples and comment on further possible extensions of these ideas. We then formulate the Wulff problem in the level set setting and use it to derive some theoretical results about Wulff shape. This method is also a convenient and versatile tool for plotting the Wulff shape of a given surface tension function in both two and three dimensions. We present numerous examples demonstrating this and verify some recently obtained theoretical results in [19] concerning the Wulff shape in the numerical section. The appendix contains proofs of some results in the main text that require certain degrees of technicality.

2. The Wulff Problem and the Legendre Transformation

This section will briefly review and develop some general results about the Wulff crystal shape that are valid in any dimension. The next section will concentrate on the Wulff crystal shape in 2D.

2.1. The Formulation of Wulff Problem. The Wulff problem is to determine the equilibrium shape of a perfect crystal of one material in contact with a single surrounding medium. The equilibrium shape is determined by minimizing the total system energy, which is composed of contributions from the bulk and surface of the crystal. If we fix the bulk energy, the problem becomes that of finding a shape of given volume with minimal surface energy.

If the surface energy density—that is, the "surface tension"—is constant, the solution is the shape of minimal surface area, which is a circle in 2D and a sphere in 3D. However, in many solid materials the surface tension depends on how the surface is directed relative to the bulk crystalline lattice, due to the detailed structure of the bonding between atoms. Assuming some standard orientation of the bulk lattice, the surface tension, γ, will be a definite function of the normal vector to the surface, $\hat{n}$, say $\gamma = \gamma(\hat{n})$. In that case, if the material is bounded by a surface Γ, the total surface energy is

$$E = \int_\Gamma \gamma(\hat{n}) dA, \tag{2.1}$$

which must be minimized subject to the constraint of constant volume enclosed by Γ.

This problem makes sense both in two and three dimensions, and essentially 2D crystals do arise experimentally in the growth of thin films [7]. The formula we derive in this section applies equally well in both dimensions. In the next section, we will concentrate our attention on the 2D problem, where we can make the precise connection to a Riemann problem. In this case, $\gamma(\hat{n})$ is the energy per unit length on the boundary, and we we seek to determine the bounding curve, Γ, of minimal surface energy that encloses a given area.

2.2. Wulff's Geometric Construction of the Solution. Wulff presented the solution to this minimization problem as an ingenious geometric construction, based on the geometry of the surface tension. Let $\gamma : S^{d-1} \to R^+$ be the surface tension which is a continuous function, where $d = 2$ or 3. Wulff's construction is as follows (refer to figure 3):

- **Step 1.** Construct a "polar plot" of $\gamma(\nu)$. In 2D, this is simply the curve defined in r-ν polar coordinates by $r = \gamma(\nu)$, $0 \le \nu \le 2\pi$. In 3D, this is a surface around the origin in sphere coordinates r-ν.
- **Step 2.** For each point P on the polar plot, construct the hyperplane through P and normal to the radial vector emanating from the origin to P. (Note this is typically *not* the tangent plane to the polar plot at P.)
- **Step 3.** Construct the inner (convex) envelope of this family of hyperplanes. This is the minimizing crystal *shape*, and rescaling it to have the proper volume yields the solution to the constrained problem.

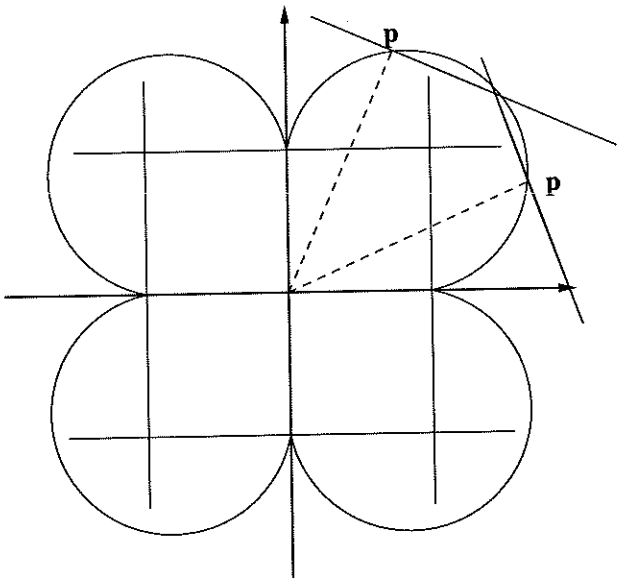

FIGURE 3. *Wulff's geometric construction.*

We will call the geometric shape obtained through the above procedure Wulff crystal shape or simply Wulff shape. It is easy to see that the region enclosed by Wulff shape is

$$W = \{\mathbf{x} \in R^d : \mathbf{x} \cdot \theta \leq \gamma(\theta), \text{ for all } \theta \in S^{d-1}\}, \tag{2.2}$$

which is convex.

It is possible to write an analytic expression for the envelope of a family of smoothly parameterized lines or planes, and doing so yields formula (2.3) in any dimension. In particular, we get a simple formula (3.1) in 2D. The stipulation from step 3 to use the "inner" envelope means that the multivalued swallowtails occurring in the envelope equations must be clipped off to obtain the true shape.

It is easy to see that the construction places facets in directions of local minima of surface tension, which is a sensible energy-reducing strategy. Indeed the entire process is simply to position a planar face at every possible orientation, with distance from the origin proportional to its energy, and then simply take the innermost set of facets as the crystal shape. However, it is difficult to prove rigorously why Wulff's construction gives the minimal energy shape. J. E. Taylor [**27**] and others [**2, 9**] have given general proofs that this construction does yield a minimizer of the energy, and this shape is unique upto translations. See also the recent paper [**19**] of Osher and Merriman.

2.3. The Wulff Shape and the Legendre Transformation. Wulff's geometric construction described above can be mathematically formalized by the use of the Legendre transformation, which we define below.

DEFINITION 1. Let $\zeta : S^{d-1} \to R^+$ be a continuous function.

1. The first Legendre transformation of ζ is:

$$\zeta_*(\nu) = \inf_{\substack{\theta \cdot \nu > 0 \\ |\theta|=1}} \left[\frac{\zeta(\theta)}{(\theta \cdot \nu)} \right]. \tag{2.3}$$

2. The second Legendre transformation of ζ is:

$$\zeta^*(\nu) = \sup_{\substack{\theta \cdot \nu > 0 \\ |\theta|=1}} \left[\zeta(\theta)(\theta \cdot \nu) \right]. \tag{2.4}$$

The geometric interpretation of Legendre transformation should be clear from figure 4 and the remarks below.

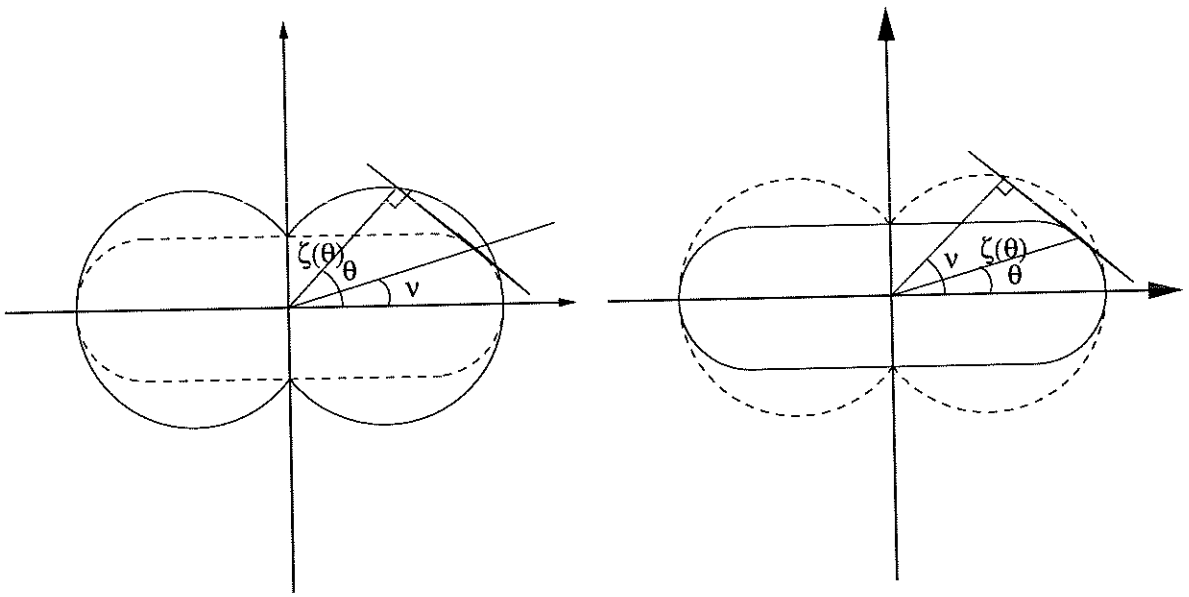

FIGURE 4. *Left: the first Legendre transformation. The solid line is the plot of ζ, and the dashed line is the plot of ζ_*, the corresponding Wulff shape. Right: second Legendre transformation. The solid line is the plot of ζ, and the dashed line is the plot of ζ^*, the support function.*

Remark 1. The first Legendre transformation $\zeta_*(\nu)$ gives the Wulff crystal shape. This is easy to see from equation (2.2) in polar coordinates:

$$\begin{aligned} W &= \{(r,\nu) : r(\nu\cdot\theta) \le \zeta(\theta), \text{ for all } \theta \in S^{d-1}\} \\ &= \{(r,\nu) : r \le \inf_{\substack{\theta\cdot\nu>0 \\ |\theta|=1}} \left[\frac{\zeta(\theta)}{(\theta\cdot\nu)}\right]\} \\ &= \{(r,\nu) : r \le \zeta_*(\nu)\}. \end{aligned}$$

Remark 2. The second Legendre transformation $\zeta^*(\nu)$ gives the support function of the region enclosed by the polar plot of ζ. Recall that the support function p_Ω of a bounded region Ω which contains the origin is defined by

$$p_\Omega(\nu) = \max\{\mathbf{x}\cdot\nu : \mathbf{x} \in \Omega\}, \text{ for } \nu \in S^{d-1}. \tag{2.5}$$

We will see shortly that the first and second Legendre transformation are dual to each other in certain sense. The following relations are obvious by definition:

LEMMA 2.1.

$$\zeta_*(\nu) \le \zeta(\nu) \le \zeta^*(\nu) \tag{2.6}$$

$$\frac{1}{\zeta^*} = \left(\frac{1}{\zeta}\right)_*, \quad \frac{1}{\zeta_*} = \left(\frac{1}{\zeta}\right)^*. \tag{2.7}$$

Since ζ is defined on a curved manifold S^{d-1}, sometimes it is convenient to study the extension of ζ to the whole R^d. We extend $\zeta : S^{d-1} \to R^+$ to R^d by defining

$$\bar{\zeta}(x) = |x|\zeta(\frac{x}{|x|}), \text{ for } x \in R^d, \text{ with } \bar{\zeta}(0) = 0. \tag{2.8}$$

Such an extension $\bar{\zeta}$ is homogeneous of degree 1. If $\bar{\zeta}$ is differentiable, we have the following important relation due to Euler:

$$\sum_{j=1}^{n} x_j \frac{\partial\bar{\zeta}}{\partial x_j}(x) = \bar{\zeta}(x). \tag{2.9}$$

Note that each of the first partial derivatives of $\bar{\zeta}$ is homogeneous of degree 0, and the second partial derivatives are homogeneous of degree -1. We will abuse the notation and write $\bar{\zeta}$ as ζ when no ambiguity arise.

DEFINITION 2. ζ is convex if the polar plot of $\frac{1}{\zeta}$ is convex. ζ is polar convex if the polar plot of ζ is convex.

The following lemma gives the necessary and sufficient condition for ζ to be convex in terms of its extension.

LEMMA 2.2. *ζ is convex if and only if its homogeneous extension of degree 1 $\bar{\zeta} : R^d \to R^+$ is a convex function on R^d.*

See Appendix I for the proof.

As we have seen, the Wulff shape $W = \{ x : |x| \le \zeta_*(\frac{x}{|x|}) \}$ is always convex. By definition, ζ_* is polar convex. From lemma 2.1, ζ^* is convex. We put these facts in

LEMMA 2.3. *ζ_* is always polar convex and ζ^* is always convex.*

Now let us introduce

$$\hat{\zeta}(\nu) = (\zeta_*)^*(\nu) \ , \ \check{\zeta}(\nu) = (\zeta^*)_*(\nu). \tag{2.10}$$

From the definitions and the lemma above, we know that $\hat{\zeta}$ is always convex and $\check{\zeta}$ polar-convex.

DEFINITION 3. We call $\hat{\zeta}(\nu)$ the Frank convexification of ζ, and $\check{\zeta}(\nu)$ the polar convexification of ζ.

We proceed to prove the following important relations:

LEMMA 2.4.

$$\hat{\zeta}(\nu) \le \zeta(\nu) \le \check{\zeta}(\nu), \tag{2.11}$$

$$\left(\frac{1}{\zeta}\right)^{\wedge} = \frac{1}{\check{\zeta}}, \quad \left(\frac{1}{\zeta}\right)^{\vee} = \frac{1}{\hat{\zeta}}. \tag{2.12}$$

Proof: From the definition,

$$\begin{aligned} \hat{\zeta}(\nu) &= \sup_{\theta\cdot\nu>0} [\zeta_*(\theta)(\theta\cdot\nu)] = \sup_{\theta\cdot\nu}[(\inf_{\eta\cdot\theta>0} \frac{\zeta(\eta)}{(\eta\cdot\theta)}(\theta\cdot\nu)] \\ &\le \sup_{\theta\cdot\nu>0} [\frac{\zeta(\nu)}{(\nu\cdot\theta)}(\theta\cdot\nu)] = \zeta(\nu). \end{aligned}$$

The other inequality can be proved similarly.

The key ingredient in proving the two equalities is the repeated use of the duality relations (2.7):

$$\begin{aligned} \left(\frac{1}{\zeta}\right)^{\wedge} &= \left(\left(\frac{1}{\zeta}\right)_*\right)^* = \left(\frac{1}{\zeta^*}\right)^* = 1/\frac{1}{\left(\frac{1}{\zeta^*}\right)^*} \\ &= 1/\left(\frac{1}{\frac{1}{\zeta^*}}\right)_* = \frac{1}{(\zeta^*)_*} = \frac{1}{\check{\zeta}}. \end{aligned}$$

The other equality follows from the above and the duality relations (2.7). □

Both $\hat{\zeta}$ and $\check{\zeta}$ have simple geometric interpretations. From the definition, the steps used to obtain $\check{\zeta}$ can be described in words as following: draw the polar-plot Γ of ζ. Let Ω be the region enclosed by Γ. Through each point on Γ, draw the hyperplane(s) tangent to Γ which lie outside Ω. Note that such a plane may not exist, such as at points that curved inward, and may not be unique, such as at the points that bulge outward. This corresponds to the steps used in constructing the support function. Then find the inner envelope of all such tangent planes. This corresponds to the construction of the Wulff shape of the support function. The inner envelope is the smallest convex set that contains Ω, i.e. the convexification of Ω. We thus get a simple procedure to obtain $\check{\zeta}$: plot the graph of ζ in polar coordinates, convexify the plot and obtain a convex graph. This is the polar plot of $\check{\zeta}$. Using the duality relation (2.12), we can obtain $\hat{\zeta}$ by first drawing the polar plot of $\frac{1}{\zeta}$, then convexifying the region enclosed to get $\left(\frac{1}{\zeta}\right)^{\vee} = \frac{1}{\hat{\zeta}}$, then inverting it to get $\hat{\zeta}$. See the figures in section 5.5. These arguments show that

LEMMA 2.5. *If ζ is convex, then $\hat{\zeta} = \zeta$. If ζ is polar-convex, then $\check{\zeta} = \zeta$.*

We now show the following important

THEOREM 2.6. 1. *The Wulff shape of ζ and $\hat{\zeta}$ are the same. That is,*

$$\left(\hat{\zeta}\right)_* = \zeta_*. \tag{2.13}$$

2. *The support function of ζ and $\check{\zeta}$ are the same. That is,*

$$\left(\check{\zeta}\right)^* = \zeta^*. \tag{2.14}$$

Proof: We already know that $\hat{\zeta} \le \zeta$. Hence $(\hat{\zeta})_* \le \zeta_*$. One the other hand,

$$\hat{\zeta}(\theta) = \max_{\substack{\theta\cdot\nu>0 \\ |\nu|=1}} [\zeta_*(\nu)(\theta\cdot\nu)] \ge \zeta_*(\nu)(\nu\cdot\theta), \text{for all } \nu \in S^{d-1}.$$

Using this inequality and the definitions, we have:

$$(\hat{\zeta})_*(\nu) = \inf_{\substack{\theta\cdot\nu>0 \\ |\theta|=1}} \left[\frac{\hat{\zeta}(\theta)}{(\theta\cdot\nu)}\right] \ge \inf_{\substack{\theta\cdot\nu>0 \\ |\theta|=1}} \left[\frac{\zeta_*(\nu)(\nu\cdot\theta)}{(\theta\cdot\nu)}\right] = \zeta_*(\nu).$$

□

From the above discussion, we see that given a convex body $K \subset R^d$, the surface tension whose Wulff shape is K is not uniquely defined. However, if we require that the surface tension is convex, then it is uniquely determined by K. If the boundary of K is given by $r : S^{d-1} \to R^+$, then the convex surface tension function whose Wulff shape is K is given by the second Legendre transformation $\gamma = r^*$.

Now let us further assume that $\zeta : S^{d-1} \to R^+$ is a C^1 function. We extend ζ to R^d to be a homogeneous function of degree 1. Then the first Legendre transformation can be rewritten as

$$\zeta_*(\theta) = \inf_{\mathbf{x}\cdot\theta>0} \left[\frac{\zeta(\mathbf{x})}{\mathbf{x}\cdot\theta}\right] = \inf_{\mathbf{x}\cdot\theta>0} \zeta\left(\frac{\mathbf{x}}{\mathbf{x}\cdot\theta}\right). \tag{2.15}$$

Suppose the infimum is reached at certain $\mathbf{x} = \mathbf{x}(\theta) \in R^d$, and let $\mathbf{p} = \frac{\mathbf{x}}{\mathbf{x}\cdot\theta}$. We have

$$\begin{aligned}
0 &= \frac{\partial}{\partial x_i}\zeta\left(\frac{\mathbf{x}}{\mathbf{x}\cdot\theta}\right) = \sum_j \frac{\partial\zeta}{\partial p_j}\frac{\partial p_j}{\partial x_i} \\
&= \sum_j \frac{\partial\zeta}{\partial p_j}\left(\frac{\delta_{ij}}{\mathbf{x}\cdot\theta} - \frac{\theta_i x_j}{(\mathbf{x}\cdot\theta)^2}\right) \\
&= \frac{\partial\zeta}{\partial p_i}\frac{1}{\mathbf{x}\cdot\theta} - \left(\sum_j \frac{\partial\zeta}{\partial p_j}p_j\right)\frac{\theta_i}{\mathbf{x}\cdot\theta} \\
&= \frac{1}{\mathbf{x}\cdot\theta}\left[\frac{\partial\zeta}{\partial p_i} - \zeta(\mathbf{p})\theta_i\right],
\end{aligned}$$

using relation (2.9). Thus we have

$$\zeta(\mathbf{p})\theta_i = \frac{\partial\zeta}{\partial p_i}(\mathbf{p}).$$

Since $\mathbf{p} = \frac{\mathbf{x}}{\mathbf{x}\cdot\theta} = \frac{\hat{n}}{\hat{n}\cdot\theta}$, where $\hat{n} = \hat{n}(\theta)$ is the unit normal to the Wulff shape at $\mathbf{R} = \zeta_*(\theta)\theta$, and $\zeta_*(\theta) = \frac{\zeta(\hat{n})}{\hat{n}\cdot\theta}$, we get

$$\zeta_*(\theta)\theta = D\zeta(\hat{n}), \tag{2.16}$$

$$\zeta_*(\theta) = |D\zeta(\hat{n})|, \tag{2.17}$$

$$\theta = \frac{D\zeta(\hat{n})}{|D\zeta(\hat{n})|}. \tag{2.18}$$

For a given θ, the $\hat{n}$ determined by (2.18) may not be unique unless ζ is strictly convex.

Equation (2.16) gives us a convenient way to get the Wulff shape for a given surface tension function γ. We simply draw the surface (in 3D) or curve (in 2D) parameterized by $\hat{n}$. The surface or curve will generally

self-intersect, except when γ is convex. We may clip off the intersecting part, and obtain the Wulff crystal shape. See next section for examples in 2D.

There are equally simple relations for the second Legendre transformation. From the duality relations (2.7), we have

$$\begin{aligned} \frac{1}{\zeta^*(\hat{n})} &= |D\frac{1}{\zeta}(\theta)|, \\ \hat{n} &= \frac{D\zeta^{-1}}{|D\zeta^{-1}|}(\theta). \end{aligned}$$

Note that here it is $1/\zeta$ that is extended as a homogeneous function of degree 1, and hence ζ itself is extended as a homogeneous function of degree -1. From the above relations, we get

$$\zeta^*(\hat{n})\hat{n} = -\frac{\zeta^2 D\zeta}{|D\zeta|^2}(\theta), \tag{2.19}$$

$$\zeta^*(\hat{n}) = \frac{\zeta^2}{|D\zeta|}(\theta), \tag{2.20}$$

$$\hat{n} = -\frac{D\zeta}{|D\zeta|}(\theta). \tag{2.21}$$

Let us look at two examples.

Example 1. In 2D, the surface tension function γ is usually given in term of the angle ν of normal $\hat{n}$ to a fixed horizontal axis, i.e. $\gamma = \gamma(\nu)$. We extend γ as a homogeneous function of degree 1 in the following way

$$\gamma(x,y) = \sqrt{x^2+y^2}\gamma(\tan^{-1}\frac{y}{x}), \tag{2.22}$$

and easily get

$$\gamma_*(\theta)\hat{n}(\theta) = D\gamma(\nu) = \gamma(\nu)\hat{n}(\nu) + \gamma'(\nu)\hat{\tau}(\nu), \tag{2.23}$$

where

$$\begin{aligned} \hat{n}(\nu) &= (\cos\nu, \sin\nu), \\ \hat{\tau}(\nu) &= (-\sin\nu, \cos\nu). \end{aligned}$$

When γ is convex, that is when $\gamma + \gamma'' \geq 0$, equation (2.23) is a parameterization of the Wulff shape in term of ν and the first Legendre transformation of γ is given by

$$\gamma_*(\theta) = \sqrt{\gamma^2(\nu) + \gamma'^2(\nu)} \tag{2.24}$$

where ν is determined by

$$\theta = \nu + \tan^{-1}\left(\frac{\gamma'(\nu)}{\gamma(\nu)}\right). \tag{2.25}$$

See section 3 for details.

To find the second Legendre transformation, we extend γ to the whole space as a homogeneous function of degree -1 by defining

$$\gamma(x,y) = \frac{1}{\sqrt{x^2+y^2}}\gamma(\tan^{-1}\frac{y}{x}). \tag{2.26}$$

From the general relations (2.19)–(2.21), we obtain

$$\gamma^*(\nu)\hat{n}(\nu) = \frac{\gamma^2(\theta)}{\gamma^2(\theta)+\gamma'^2(\theta)}[\gamma(\theta)\hat{n}(\theta) - \gamma'(\theta)\hat{\tau}(\theta)], \tag{2.27}$$

$$\gamma^*(\nu) = \frac{\gamma^2(\theta)}{\sqrt{\gamma^2(\theta)+\gamma'^2(\theta)}}, \tag{2.28}$$

where θ is determined by

$$\nu = \theta - \tan^{-1}\left(\frac{\gamma'(\theta)}{\gamma(\theta)}\right). \tag{2.29}$$

Example 2. In 3D, suppose the surface tension function is given in terms of spherical coordinates, $\gamma = \gamma(\nu, \psi)$, where $0 \le \nu < 2\pi$ and $-\frac{\pi}{2} < \psi < \frac{\pi}{2}$. We extend γ to the whole space by defining

$$\gamma(x, y, z) = \sqrt{x^2 + y^2 + z^2}\, \gamma(\tan^{-1}\frac{y}{x}, \tan^{-1}\frac{z}{\sqrt{x^2 + y^2}}), \tag{2.30}$$

and direct calculation gives:

$$D\gamma = \gamma(\nu, \psi)\hat{r} + \frac{1}{\cos\psi}\frac{\partial\gamma}{\partial\nu}\hat{\nu} + \frac{\partial\gamma}{\partial\psi}\hat{\psi}, \tag{2.31}$$

where

$$\begin{aligned} \hat{r} &= (\cos\psi\cos\nu, \cos\psi\sin\nu, \sin\psi), \\ \hat{\nu} &= (-\sin\nu, \cos\nu, 0), \\ \hat{\psi} &= (-\sin\psi\cos\nu, -\sin\psi\sin\nu, \cos\psi). \end{aligned}$$

Equation (2.31) is a parameterization of Wulff shape in terms of ν and ψ when γ is convex. The first Legendre transformation is given by

$$\gamma_*(\theta, \phi) = \sqrt{\gamma^2(\nu, \psi) + \left|\frac{1}{\cos\psi}\frac{\partial\gamma}{\partial\nu}\right|^2 + \left|\frac{\partial\gamma}{\partial\psi}\right|^2}, \tag{2.32}$$

where ν and ψ are implicitly defined by equation (2.18).

2.4. Growing a Wulff Crystal. Now we consider a surprising and interesting property of objects moving outward with normal velocity equal to the surface tension function γ. This is discussed in more detail in section 7.3 below.

In [19], Osher and Merriman proved a generalization of a conjecture made by Chernov [4, 5]. Namely, starting from any (not necessarily convex or even connected) region, if we grow it with normal velocity equal to (not necessarily convex) $\gamma(\nu) : S^{d-1} \to R^+$, where $\nu \in S^{d-1}$ is the unit normal direction, the region asymptotes to a single Wulff shape corresponding to the surface tension γ. This is not totally surprising, because if we start with a convex region whose support function is $p(\nu)$ and move it outward with normal velocity $\gamma(\nu)$, with $\gamma(\nu)$ convex, the evolution of $p(\nu, t)$, the support function of the growing region at time t, satisfies:

$$\begin{cases} \frac{\partial p}{\partial t}(\nu, t) = \gamma(\nu), \\ p(\nu, 0) = p(\nu). \end{cases} \tag{2.33}$$

Thus the evolving region has support function

$$p(\nu, t) = p(\nu) + t\gamma(\nu),$$

so the growing region asymptotes to the Wulff shape associated with $\gamma(\nu)$. This argument is only valid for convex initial shape and convex γ. In particular, it shows that a growing Wulff shape under this motion just expands itself similarly, since $p(\nu) = \gamma(\nu)$ for a convex γ. This is also true for a nonconvex γ. See [19] and section 7.3 below for more details.

2.5. Typical Forms for Surface Tension. From Wulff's construction, we see that the crystalline form depends on the geometry of the polar plot of the surface tension. While Wulff's construction is valid for an arbitrary surface tension function, the polar plots of physically relevant surface tensions have several characteristic features. These are worth noting in order to appreciate the crystalline forms in nature and also in order to formulate representative examples.

A physical surface tension should have reflection symmetry, $\gamma(\hat{n}) = \gamma(-\hat{n})$. Further, it is known that modeling a crystalline material as a regular lattice of atoms with given bonding energies between neighbors necessarily leads to a continuum limit in which the polar plot of γ consists of portions of spheres (circles in 2D) passing through the origin [10]. In particular, a 2D plot consists of outward bulging circular arcs that meet at inward pointing cusps. A simple example coming from a square lattice (X-Y) model of a 2D crystal is $\gamma(\nu) = |\sin(\nu)| + |\cos(\nu)|$. The polar plot consists of four semicircular arcs arranged in a clover-leaf fashion. The cubic lattice (X-Y-Z) model of a 3D crystal is $\gamma(\hat{n}) = |\hat{n}_x| + |\hat{n}_y| + |\hat{n}_z|$. Its plot in spherical coordinates consists of eight spherical pieces in a similar fashion. Its Wulff shape is a cube. See figure 5.

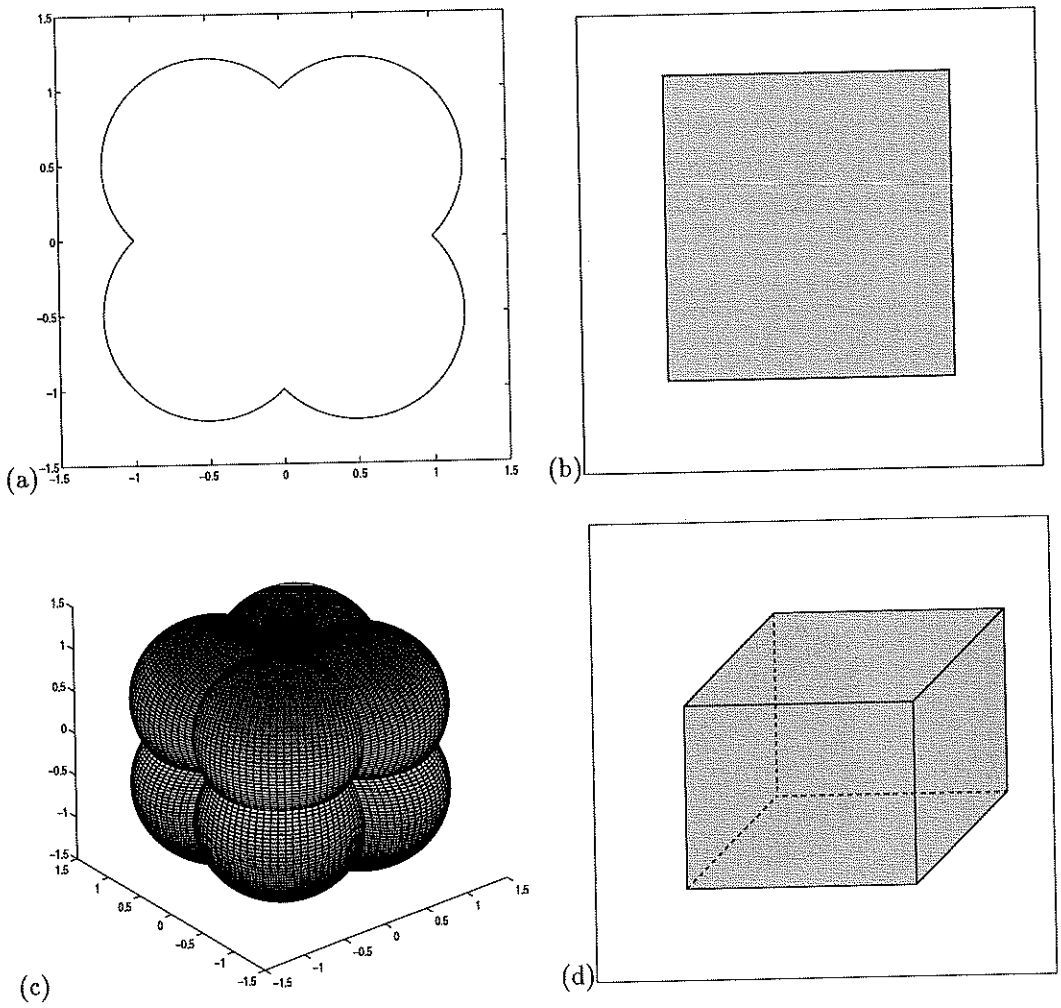

FIGURE 5. *(a) Plot of* $\gamma(\nu) = |\cos\nu| + |\sin\nu|$. *(b) Wulff shape of* γ *on the left. (c) Plot of* $\gamma(\hat{n}) = |\hat{n}_x| + |\hat{n}_y| + |\hat{n}_z|$. *(d) Wulff shape of* γ *on the left.*

Physical surface tensions depend on the material temperature as well, and increasing temperature tends to smooth out the cusps in the surface tension plot.

From Wulff's construction, we can see that each cusp in the γ plot will result in a facet on the crystal shape. Increasing the material temperature smoothes out the cusps, which in turn rounds out the original facets of the Wulff shape.

3. The Wulff Crystal Shape in 2D

In 2D, a unit vector can be represented by its angle to a horizontal axis. Many of the general results developed in the last section have interesting concrete expressions. Although we can obtain many of the results in this section by a simple change of variables and then apply the general results, as we did in the example above, we will see that 2D Wulff problem has its own fascinating properties which may be missed by this "general-to-special" approach. Instead, we will use the general results as a guideline and develop the 2D theory from the ground up. A comprehensive discussion of the 2D Wulff problem and related matters can be found in the book of Gurtin [**11**].

Choosing the angle between the outward unit normal to the horizontal axis as parameter, the 2D version of the Legendre transformations of a function $\zeta : S^1 \to R^+$ are

$$\zeta_*(\theta) = \inf_{\theta-\frac{\pi}{2}<\nu<\theta+\frac{\pi}{2}} \left[\frac{\zeta(\nu)}{\cos(\theta-\nu)}\right], \tag{3.1}$$

$$\zeta^*(\theta) = \sup_{\theta-\frac{\pi}{2}<\nu<\theta+\frac{\pi}{2}} [\zeta(\nu)\cos(\theta-\nu)]. \tag{3.2}$$

3.1. The Legendre Transformation in 2D. We briefly review some basic facts about plane curves. For convenience, we will change the notation of the Legendre transformation in the section. Given $r : S^1 \to R^+$, a continuous function. Let $\mathbf{r} : S^1 \to R^2$ be the polar plot of r, i.e. $\mathbf{r}(\theta) = r(\theta)(\cos\theta, \sin\theta)$, and denote the resulting curve as Γ. The second Legendre transformation of r is the support function of Γ and will be denoted as p. One the other hand, given a positive continuous function $p : S^1 \to R^+$, its first Legendre transformation gives the Wulff shape and will be denoted as r.

We will use s to denote the arclength parameter of Γ, and θ the angle between $\mathbf{r}$ and the horizontal x-axis. Let $\hat{\tau} = \frac{d\mathbf{r}}{ds}$ be the tangent vector and $\hat{n}$ be the outwards unit normal. Let $\nu \in [0, 2\pi)$ be the angle between $\hat{n}$ and x-axis.Then $\hat{n} = (\cos\nu, \sin\nu), \hat{\tau} = (-\sin\nu, \cos\nu)$.

The curvature of the curve Γ has a simple expression in term of ν:

$$\kappa = \frac{d\nu}{ds}. \tag{3.3}$$

Recall that the support function of the curve Γ is defined as

$$p(\nu) = \max_{\theta}\{\mathbf{r}(\theta)\cdot\hat{n}(\nu)\}. \tag{3.4}$$

Suppose the maximum is obtained at $\theta = \theta(\nu)$. Differentiate with respect to ν, we get:

$$p'(\nu) = \mathbf{r}(\theta)\cdot\hat{\tau}(\nu). \tag{3.5}$$

Note that $\mathbf{r} = (\mathbf{r}\cdot\hat{n})\hat{n} + (\mathbf{r}\cdot\hat{\tau})\hat{\tau}$. Combining the definition of p and the above equation, we get

$$\mathbf{r}(\theta) = p(\nu)\hat{n}(\nu) + p'(\nu)\hat{\tau}(\nu), \tag{3.6}$$

which gives us a simple way to express the curve if we know its support function.

Differentiating equation (3.5) with respect to ν gives

$$p''(\nu) = \frac{1}{\kappa} - p(\nu), \tag{3.7}$$

or equivalently:

$$\kappa = \frac{1}{p(\nu)+p''(\nu)}. \tag{3.8}$$

This gives us a convenient way to express the curvature of a curve given its support function.

Recall from the last section that for a positive function on S^1 to be a support function, it must be convex in the sense that the polar plot of its reciprocal be convex. The curvature of the polar plot of $1/p$ is easily shown to be

$$\kappa = \frac{p^3(p+p'')}{(p^2+p'^2)^{3/2}}. \tag{3.9}$$

Thus p is convex if and only if $p + p'' \geq 0$.

From the above results, we can find explicit formulae for the first and second Legendre transformations in 2D. Given $p : S^1 \to R^+$, its first Legendre transformation $r(\theta) = p_*(\theta)$ is simply:

$$r(\theta) = \sqrt{p^2(\nu)+p'^2(\nu)}. \tag{3.10}$$

To determine ν for a given θ, let

$$\alpha = \tan^{-1}\left(\frac{p'(\nu)}{p(\nu)}\right). \tag{3.11}$$

We have

$$\begin{aligned}\mathbf{r}(\theta) &= r(\theta)\left[\frac{p(\nu)}{r(\theta)}\hat{n}(\nu)+\frac{p'(\nu)}{r(\theta)}\hat{\tau}(\nu)\right]\\ &= r(\theta)(\cos(\alpha+\nu),\sin(\alpha+\nu)).\end{aligned}$$

So

$$\theta = \nu + \tan^{-1}\left(\frac{p'(\nu)}{p(\nu)}\right), \tag{3.12}$$

which implicitly defines ν for a given θ. To ensure the inverse exists, we need

$$\frac{\partial\theta}{\partial\nu} = \frac{p(p+p'')}{p^2+p'^2} \geq 0,$$

or equivalently

$$p(\nu)+p''(\nu) \geq 0. \tag{3.13}$$

That is to say, p has to be convex.

On the other hand, suppose we are given $r : S^1 \to R^+$. To find its second Legendre transformation, i.e. its support function p, we note that

$$\mathbf{r}'(\theta) = r'(\theta)\hat{n}(\theta) + r(\theta)\hat{\tau}(\theta).$$

Define

$$\beta = \tan^{-1}\left(\frac{r'(\theta)}{r(\theta)}\right). \tag{3.14}$$

We have the following expression for the tangent vector at $\mathbf{r}(\theta)$

$$\begin{aligned}\hat{\tau}(\nu) &= \frac{\mathbf{r}'(\theta)}{|\mathbf{r}'(\theta)|} = \sin\beta\hat{n}(\theta)+\cos\beta\hat{\tau}(\theta)\\ &= (-\sin(\theta-\beta),\cos(\theta-\beta)).\end{aligned}$$

Thus

$$\nu = \theta - \tan^{-1}\left(\frac{r'(\theta)}{r(\theta)}\right), \tag{3.15}$$

which determines θ for a given ν. To ensure that the inverse exists, we require

$$\frac{\partial\nu}{\partial\theta} = \frac{r^2+2|r'|^2-r''r}{r^2+|r'|^2} = \frac{R(R+R'')}{R^2+|R'|^2} \geq 0,$$

or equivalently

$$R(\theta)+R''(\theta) \geq 0,$$

where $R = \frac{1}{r}$. This is equivalent to that r is polar convex.

The support function is found to be

$$\begin{aligned}p(\nu) &= \mathbf{r}(\theta)\cdot\hat{n}(\nu) = r(\theta)\hat{n}(\theta)\cdot\hat{n}(\nu)\\ &= r(\theta)\cos(\theta-\nu) = r(\theta)\cos(\beta)\\ &= \frac{r^2(\theta)}{\sqrt{r^2(\theta)+r'^2(\theta)}},\end{aligned}$$

and

$$\begin{aligned}\mathbf{p}(\nu) &= p(\nu)(\cos(\theta-\beta),\sin(\theta-\beta))\\ &= \frac{r^2(\theta)}{r^2(\theta)+r'^2(\theta)}\left[r(\theta)\hat{n}(\theta)-r'(\theta)\hat{\tau}(\theta)\right],\end{aligned}$$

where θ is defined by equation (3.15).

We summarize the results in this section in the following

THEOREM 3.1. 1. *Given $p : S^1 \to R^+$, a continuous piecewise differentiable convex function, its first Legendre transformation is*

$$r(\theta) = \sqrt{p^2(\nu) + p'^2(\nu)}$$

and

$$\mathbf{r}(\theta) = p(\nu)\hat{n}(\nu) + p'(\nu)\hat{\tau}(\nu),$$

where ν is determined by

$$\theta = \nu + \tan^{-1}\left(\frac{p'(\nu)}{p(\nu)}\right)$$

for a given θ.

2. *Given $r : S^1 \to R^+$, a continuous piecewise differentiable polar convex function, its second Legendre transformation is*

$$p(\nu) = \frac{r^2(\theta)}{\sqrt{r^2(\theta) + r'^2(\theta)}}$$

and

$$\mathbf{p}(\nu) = \frac{r^2(\theta)}{r^2(\theta) + r'^2(\theta)}\left[r(\theta)\hat{n}(\theta) - r'(\theta)\hat{\tau}(\theta)\right],$$

where θ is determined by

$$\nu = \theta - \tan^{-1}\left(\frac{r'(\theta)}{r(\theta)}\right)$$

for a given ν.

3.2. The Euler-Lagrange Equation. We can apply standard variational calculus to obtain the Euler-Lagrange equations for the minimizing boundary curve in the 2D problem. For our purposes, these equations are best expressed when the curve is parameterized in terms of the angle, ν, between its unit normal vector and some fixed axis, as a function of arc length s along the curve, as was done in the previous section. The curve is completely specified by $\nu(s)$.

In this parameterization, the Euler-Lagrange equation become

$$(\gamma(\nu) + \gamma''(\nu))\nu_s = \lambda, \tag{3.16}$$

where λ is the constant Lagrange multiplier associated with the volume constraint. It is worth noting that $\nu_s = \kappa$, the curvature of the curve; in particular, this shows that when the surface tension is constant, the solution is of constant curvature, i.e. a circle.

For the derivation of the Euler-Lagrange equation of the surface energy, which contains (3.16) as a special case, see Appendix III.

3.3. Multivalued Solutions. Equation (3.6) give us a simple ways to obtain the Wulff shape given the surface tension function γ. We can represent the Wulff shape of γ using ν as parameter:

$$\mathbf{x}(\nu) = \gamma(\nu)\hat{n}(\nu) + \gamma'(\nu)\hat{\tau}(\nu). \tag{3.17}$$

This is true only when γ is convex, i.e. $\gamma + \gamma'' \geq 0$. In this case, the curve Γ defined by $\mathbf{x}(\nu)$ is convex. When the convexity condition fails, the curve will self-intersect and thus have swallowtails. See figure 6. This can be easily seen by noting that

$$\mathbf{x}'(\nu) = (\gamma(\nu) + \gamma''(\nu))\hat{\tau}(\nu). \tag{3.18}$$

It is clear that the curve kinks and reverses direction whenever $\gamma(\nu) + \gamma''(\nu)$ changes sign, as it does at each corner of a swallowtail. Suppose the curve $\mathbf{x}$ self-intersects at $\nu = \nu_L$ and $\nu = \nu_R$, then the following condition must be satisfied

$$\gamma(\nu_L)\hat{n}(\nu_L) + \gamma'(\nu_L)\hat{\tau}(\nu_L) = \gamma(\nu_R)\hat{n}(\nu_R) + \gamma'(\nu_R)\hat{\tau}(\nu_R). \tag{3.19}$$

In this case, we can obtain the Wulff shape simply by clipping off the swallowtail.

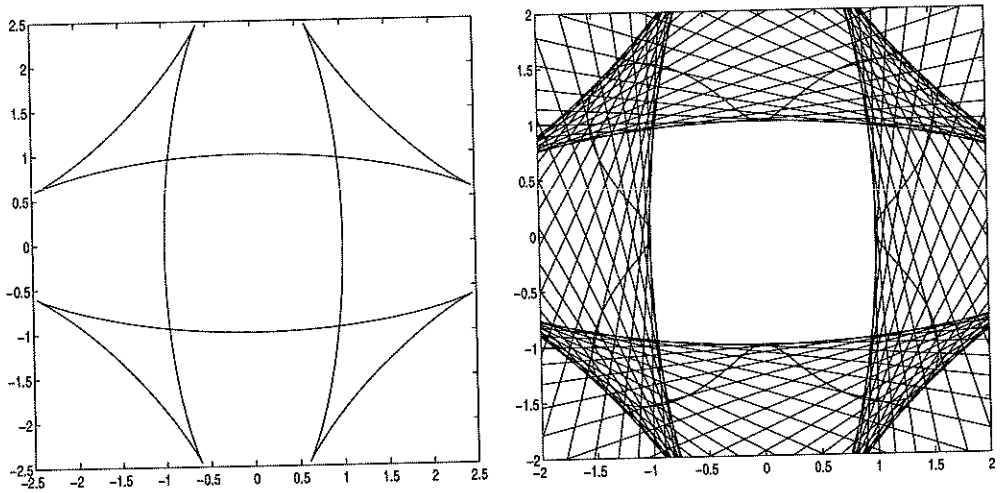

FIGURE 6. *Left: Plot of formula (3.17) when* $\gamma(\nu) = 1+\sin^2(2\nu)$. *Swallowtails appear since this* γ *is not convex. Right: Wulff shape from Wulff's geometric construction. Notice that by clipping off the swallowtails in the graph on the left, we get the true Wulff shape.*

There is yet another way to obtain the Wulff shape from γ. The Euler-Lagrange equation can be written as a simple first order ordinary differential equation (taking λ as 1, which is amounts to a rescaling of the length of the curve Γ)

$$\frac{d\nu}{ds} = \frac{1}{(\gamma(\nu)+\gamma''(\nu))}, \tag{3.20}$$

which completely specifies the curve up to a scaling.

If $\gamma+\gamma''$ does not change sign, there are two possibilities. If $\gamma+\gamma''$ stays positive, the right hand side is always finite and can be integrated to compute a convex shape (since the curvature $\kappa = \nu_s$ is positive). This is the unique solution to Wulff's problem. If $\gamma+\gamma'' \geq 0$, and becomes 0 at some points, the resulting curve is still convex, and yet has kinks at points where $\gamma+\gamma''$ vanishes.

However, if $\gamma+\gamma''$ does change sign, the curve one obtains from this integration will not be convex, can have kinks (points where curvature $\kappa = \nu_s$ is infinite), and will typically cross over itself, so that it does not even define a possible material shape. The result can be considered as a multiple valued solution to the problem, since in polar coordinates with origin at the crystal center it corresponds to having a multivalued radius as a function of polar angle. This multivalued solution can be regularized to obtain the desired solution by "clipping off" the non-physical parts of the shape created by self-crossings.

3.4. Frank's Convexification of Surface Tension. Many different surface tension functions can lead to the same Wulff shape. This is clear from Wulff's geometric construction, which effectively ignores the behavior of the parts of the γ polar plot farthest from the origin, i.e. the high energy parts of the surface tension function. Thus in general we have the freedom of using a surface tension that is *equivalent* to the original γ, in the sense that it has the same Wulff shape.

The breakdown of equation (3.17) and (3.20) ultimately stems from a change in sign of $\gamma+\gamma''$. We would thus like to use our freedom to define an equivalent surface tension, $\hat{\gamma}$, for which

$$\hat{\gamma}+\hat{\gamma}'' \geq 0. \tag{3.21}$$

It turns out there is a classical procedure known as Frank convexification which yields such an equivalent surface tension.

The Frank convexification of γ, denoted $\hat{\gamma}$, involves two Legendre transformations and appears complicated. See formula (2.10) in section 2.3. But there exists a simple geometric procedure to obtain $\hat{\gamma}$ from γ by taking the polar plot of $1/\gamma(\nu)$, forming its outer convex hull, and defining this to be the polar plot of $1/\hat{\gamma}(\nu)$. The results in section 2.3 shows that the relationship between the surface tension plot and the Wulff shape becomes a standard geometric duality when viewed under the inversion mapping. See also the article of Frank [10].

Now let us take a closer look at the above procedure. The normal direction to the curve $r(\nu) = \frac{1}{\gamma(\nu)}$ is

$$\theta = \nu + \tan^{-1}\left(\frac{\gamma'(\nu)}{\gamma(\nu)}\right). \tag{3.22}$$

Thus

$$\theta_\nu = \frac{\gamma(\gamma + \gamma'')}{\gamma^2 + \gamma'^2}. \tag{3.23}$$

The curve fails to be convex only when $\gamma + \gamma'' < 0$. There are basically two situations where this can happen. One situation is that there is a region on the plot of $r = \gamma(\nu)$ that "bumps" out. For the plot of $r = \frac{1}{\gamma(\nu)}$, it corresponds to a region that curves inward. Thus the convexifying curve $r = \frac{1}{\hat{\gamma}(\nu)}$ is a straight line, tangent to the curve $r = \frac{1}{\gamma(\nu)}$ at two points $(\nu_L, \frac{1}{\gamma(\nu_L)})$ and $(\nu_R, \frac{1}{\gamma(\nu_R)})$. The other situation is that the plot of $r = \gamma(\nu)$ has a inward cusp at $\nu = \nu_M$. Then the curve $r = \frac{1}{\gamma(\nu)}$ has a kink at $\nu = \nu_M$, and this curve can be convexified by two lines which meet at the tip $(\nu_M, \frac{1}{\gamma(\nu_M)})$, and are tangent to the curve at two points $(\nu_L, \frac{1}{\gamma(\nu_L)})$ and $(\nu_R, \frac{1}{\gamma(\nu_R)})$. See figure 7.

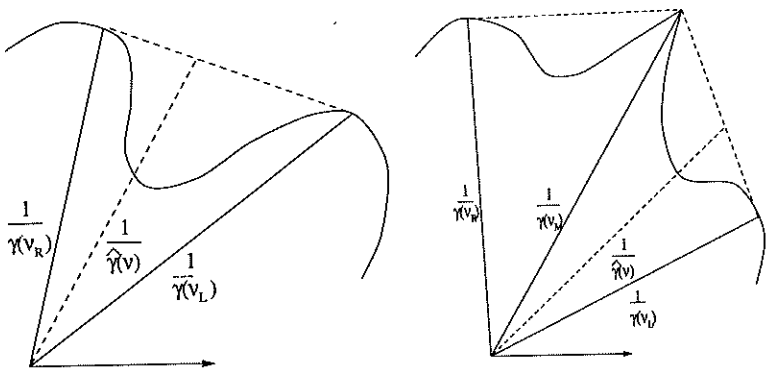

FIGURE 7. *Left: the first case; Right: the second case.*

In the first case, the polar plot of $\hat{\gamma}$ contains a circular arc whose extension passes through the origin and

$$\hat{\gamma}(\nu) = \frac{\gamma(\nu_R)\sin(\nu - \nu_L) + \gamma(\nu_L)\sin(\nu_R - \nu)}{\sin(\nu_R - \nu_L)}, \text{ for } \nu_L \le \nu \le \nu_R. \tag{3.24}$$

One can easily derive the following jump conditions

$$\gamma(\nu_L)\cos\nu_L - \gamma'(\nu_L)\sin\nu_L = \gamma(\nu_R)\cos\nu_R - \gamma'(\nu_R)\sin\nu_R, \tag{3.25}$$

$$\gamma(\nu_L)\sin\nu_L + \gamma'(\nu_L)\cos\nu_L = \gamma(\nu_R)\sin\nu_R + \gamma'(\nu_R)\cos\nu_R \tag{3.26}$$

from the second order contact of the line with the original curve. Note that these equations are exactly the self-intersection condition (3.19).

In the second case, the polar plot of $\hat{\gamma}$ has two circular arcs and meet at $\nu = \nu_M$ and form a cusp there, and we have

$$\hat{\gamma}(\nu) = \frac{\gamma(\nu_L)\sin(\nu_M - \nu) + \gamma(\nu_M)\sin(\nu - \nu_L)}{\sin(\nu_M - \nu_L)}, \text{ for } \nu_L \le \nu \le \nu_M, \tag{3.27}$$

$$\hat{\gamma}(\nu) = \frac{\gamma(\nu_M)\sin(\nu_R - \nu) + \gamma(\nu_R)\sin(\nu - \nu_M)}{\sin(\nu_R - \nu_M)}, \text{ for } \nu_M \le \nu \le \nu_R. \tag{3.28}$$

At ν_M the convexified surface tension $\hat{\gamma}$ is continuous and $\hat{\gamma}(\nu_M) = \gamma(\nu_M)$, but γ and $\hat{\gamma}$ each have a jump in derivative there. The following inequalities are satisfied:

$$\gamma'(\nu_M^-) \le \hat{\gamma}'(\nu_M^-) < 0 < \hat{\gamma}'(\nu_M^+) \le \gamma'(\nu_M^+), \tag{3.29}$$

where

$$\hat{\gamma}'(\nu_M^-) = \frac{\gamma(\nu_M)\cos(\nu_L - \nu_M) - \gamma(\nu_L)}{\sin(\nu_M - \nu_L)},$$
$$\hat{\gamma}'(\nu_M^+) = \frac{\gamma(\nu_R) - \gamma(\nu_M)\cos(\nu_L - \nu_M)}{\sin(\nu_R - \nu_M)}.$$

In both cases, we have the following inequality

$$\gamma(\nu) \geq \hat{\gamma}(\nu), \text{ for } \nu_L \leq \nu \leq \nu_R. \tag{3.30}$$

We note that when this convexified surface tension is used within the general formula (3.17) for the multivalued solution to Wulff's problem, the resulting curve

$$\mathbf{x}(\nu) = \hat{\gamma}(\nu)\hat{n}(\nu) + \hat{\gamma}'(\nu)\hat{\tau}(\nu) \tag{3.31}$$

has no self-intersections and thus is the correct Wulff shape. In the first case discussed above, $\hat{\gamma}(\nu)+\hat{\gamma}''(\nu) = 0$ on $[\nu_L, \nu_R]$, thus the Wulff shape defined by (3.31) has a sharp corner where the normal jumps from ν_L to ν_R. In the second case, $\hat{\gamma}(\nu)+\hat{\gamma}''(\nu) = 0$ on $[\nu_L, \nu_M)$ and $(\nu_M, \nu_R]$ and $\hat{\gamma}(\nu_M)+\hat{\gamma}(\nu_M) = \infty$. The normal to the Wulff shape jumps from ν_L to ν_M, forming a corner there, then stays equal to ν_M and forms a facet, and then jumps again from ν_M to ν_R, forming another corner. Thus the second case corresponds to two corners connected with a facet.

The Frank convexified surface tension provides the basis for our general Riemann problem representation of the Wulff shape.

3.5. Two Formulae for the Normal Direction. Recall that the Wulff shape is given by the first Legendre transformation

$$\gamma_*(\theta) = \inf_{\theta - \frac{\pi}{2} < \nu < \theta + \frac{\pi}{2}} \left[\frac{\gamma(\nu)}{\cos(\theta - \nu)} \right].$$

So the problem of finding the Wulff shape for a given γ is reduced to find the $\nu(\theta)$ for a given θ where the infimum is reached. This section concerns finding explicit formulae for $\nu(\theta)$ which we will see shortly is closely connected with the Riemann problem for a scalar conservation law.

We point out some technical difficulties here. First of all, for a given θ, there may exist more than one ν that minimizes $\frac{\gamma(\nu)}{\cos(\theta-\nu)}$. This occurs partly because γ may not be convex. We can get rid of this difficulty by replacing γ by $\hat{\gamma}$, since γ and $\hat{\gamma}$ have the same Wulff shape. But even if this convexity condition is satisfied, there is still no uniqueness when $\gamma(\nu)+\gamma''(\nu) = 0$. Such a situation arise at the corner of a Wulff shape. We deal with this ambiguity by requiring $\nu(\theta)$ to be increasing and continuous from the right in θ. Secondly, it is a subtle matter how to choose the range for the normal angle ν and the polar angle θ of the convex Wulff shape so that under the above assumptions on γ and $\nu(\theta)$, the one to one correspondence between ν and θ is naturally defined. This can be achieved by choosing the horizontal axis so that it intersects with the Wulff shape at a (global) minima of the surface tension. At this point, both the normal angle and the polar angle are 0 or 2π. Since the Wulff shape is convex, $\nu(\theta)$ must be a nondecreasing function in θ. Thus the ν–θ correspondence can be chosen as a function from $[0, 2\pi]$ to itself. This will be our choice of horizontal axis in our theoretical analysis below.

Our first expression of $\nu(\theta)$ is

LEMMA 3.2. *For each $\theta \in [0, 2\pi)$, there is a unique $\nu = \nu(\theta)$ that is increasing, continuous from the right and is implicitly defined by*

$$\theta = \nu + \tan^{-1}\left(\frac{\hat{\gamma}'(\nu)}{\hat{\gamma}(\nu)}\right). \tag{3.32}$$

We postpone the proof and introduce

DEFINITION 4.

$$F(\nu) = \frac{1}{2}\nu^2 + \int_0^\nu \tan^{-1}\left(\frac{\hat{\gamma}'(u)}{\hat{\gamma}(u)}\right) du. \tag{3.33}$$

We notice that

$$F'(\nu) = \nu + \tan^{-1}\left(\frac{\hat{\gamma}'(\nu)}{\hat{\gamma}(\nu)}\right), \tag{3.34}$$

$$F''(\nu) = \frac{\hat{\gamma}(\nu)(\hat{\gamma}(\nu)+\hat{\gamma}''(\nu))}{\hat{\gamma}^2(\nu)+\hat{\gamma}'^2(\nu)}. \tag{3.35}$$

Since $\theta = F'(\nu) \geq 0$ and $\hat{\gamma} + \hat{\gamma}'' \geq 0$, F is always nondecreasing and convex.
Our second expression for $\nu(\theta)$ is

THEOREM 3.3.

$$\nu(\theta) = -\frac{d}{d\theta} \min_{0\leq\nu\leq 2\pi} [F(\nu) - \theta\nu]. \tag{3.36}$$

We outline the proof of the above two results here. Refer to figure 8 to get the idea. Lemma 3.2 follows from the fact that $F'(\nu)$ is an increasing function in ν and formula (3.12).

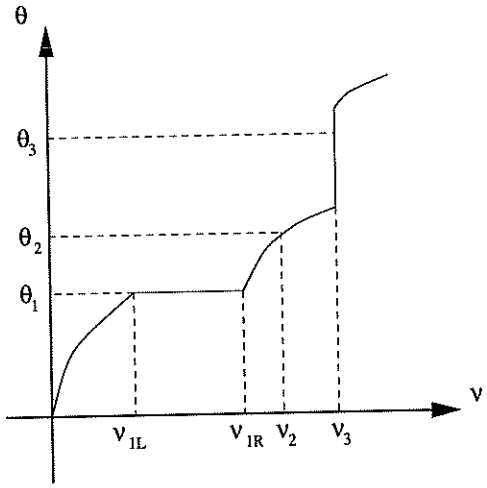

FIGURE 8. *Plot of* $\theta = F'(\nu)$ *vs* ν.

To prove Theorem 3.3, suppose the infimum of $F(\nu) - \theta\nu$ is reached at $\tilde{\nu}$. The first order condition

$$\frac{d}{d\nu}[F(\nu) - \theta\nu] \mid_{\nu=\tilde{\nu}} = F'(\tilde{\nu}) - \theta = 0$$

gives

$$\theta = \tilde{\nu} + \tan^{-1}\left(\frac{\hat{\gamma}'(\tilde{\nu})}{\hat{\gamma}(\tilde{\nu})}\right).$$

So $\tilde{\nu} = \nu(\theta)$ except at points where $F'(\nu) = \theta$ over some interval $\nu \in [\nu_L, \nu_R]$. (As a function of θ, ν jumps from ν_L to ν_R.) Such θ are isolated. Ignoring this situation, we have

$$\begin{aligned} \text{rhs} &= -\frac{d}{d\theta}[F(\nu(\theta)) - \theta\nu(\theta)] \\ &= -F'(\nu(\theta))\nu'(\theta) + \nu(\theta) + \theta\nu'(\theta) \\ &= \nu(\theta). \end{aligned}$$

So our result is valid except at countable isolated points. The values of $\nu(\theta)$ at the jumps are uniquely determined by the requirement that ν is increasing and continuous from the right.

4. The Riemann Problem

4.1. The Riemann Problem Formulation. The original Riemann problem was to determine the 1D dynamics of a gas when the initial data consists of constant states to the left and right separated by a single discontinuous jump in value.

The equations of motion for a gas are generally formulated as integral conservation laws for mass, momentum and energy. In one spatial dimension (1D), these state that the rate of change of the amount of conserved quantity contained in any interval $[x_1, x_2]$ is due to the difference between the flux out at x_2 and the flux in at x_1:

$$\frac{d}{dt}\int_{x_1}^{x_2} u(x,t)dx = f(u(x_2,t)) - f(u(x_1,t)), \tag{4.1}$$

where $u(x,t)$ is the density of the conserved quantity, and $f(u)$ is the corresponding flux function.

When the solution u is smooth, by letting $x_1 - x_2$ become infinitesimal these integral conservation laws can be reduced to differential equations. The result is a system of hyperbolic conservation laws of the form

$$u_t + f(u)_x = 0 \tag{4.2}$$

for the conservative convective transport of mass, momentum and energy.

Riemann's problem was to find the solution of equation (4.2) for arbitrary piecewise constant initial data

$$u = u_L, x < 0, \tag{4.3}$$

$$u = u_R, x > 0, \tag{4.4}$$

where u_L and u_R are the constant states to the left and right of the origin.

The problem as posed is physically idealized, since the conservation law (4.2) does not include any viscous or diffusive transport effects. In a real gas the viscous effects are usually small, but they do play a role when the states have steep spatial gradients as in the Riemann problem. Indeed, it turns out that idealized Riemann problem allows multiple solutions. The unique physically relevant one is the "viscosity solution", i.e. the limiting solution as viscosity goes to zero $u = \lim_{\epsilon \downarrow 0} u^\epsilon$ from the viscous version of the conservation law:

$$u_t^\epsilon + f(u^\epsilon)_x = \epsilon u_{xx}^\epsilon. \tag{4.5}$$

In contrast, this regularized equation has unique well behaved solutions for any $\epsilon > 0$.

Both the Riemann problem and the viscosity solution make sense for general systems of hyperbolic conservation laws, and the names commonly refer to this more general context. The Riemann problem solutions provide insight into the fundamental propagation of discontinuities in the system. For our purposes, we will only need to consider a single conservation equation, so that u is a scalar state, with scalar flux $f(u)$.

A comprehensive discussion of the the Riemann problem for gas dynamics and related matters can be found in the text of Courant and Friedrichs [6].

4.2. Multiple-Valued Solutions. The solutions to the Riemann problem have a simple form in which a disturbance emanates from initial discontinuity at $x = 0$. These solutions can be found by assuming the time self-similar form $u(x,t) = u(x/t)$, which implies the graph of $u(x,t)$ has the same shape at all times, differing only by a spatial rescaling. Substituting this form into the conservation law 4.2 results in the equation

$$(-\theta + f'(u))u_\theta = 0, \tag{4.6}$$

where $\theta = x/t$ is the similarity variable. The formal solution consists of regions on the left and right where u is constant with values u_L and u_R, joined by a region in which $u(\theta) = (f')^{-1}(\theta)$. If $f''(u)$ changes sign between u_L and u_R, then the inverse of f' is multivalued and this u can be considered a multivalued solution of the Riemann problem.

Such a multivalued solution is not physically meaningful, so some additional principle is required to extract a single valued solution by "clipping off" extra values. However, from a plot of the multivalued solution it is not immediately obvious where to clip.

The proper single-valued, self-similar solution to the Riemann problem is given analytically by

$$u(\theta) = -\frac{d}{d\theta} \min_{u_L \le u \le u_R} (f(u) - \theta u), \text{ if } u_L \le u_R. \tag{4.7}$$

$$u(\theta) = -\frac{d}{d\theta} \max_{u_L \ge u \ge u_R} (f(u) - \theta u), \text{ if } u_L \ge u_R. \tag{4.8}$$

This formula was first derived by Osher in [15] and [16]; It can be understood as an analytical interpretation of the geometric construction given in the next section.

Note that in (4.7) f can be replaced by the convexified $\hat{f}$. In the case when $u_L < u_R$, $\hat{f}$ is defined by

$$f_*(\theta) = \min_{u_L \le u \le u_R} [f(u) - \theta u], \tag{4.9}$$

$$\hat{f}(u) = \max_{-\infty < \theta < \infty} [f_*(\theta) + \theta u]. \tag{4.10}$$

The case $u_L > u_R$ can be defined similarly.

It follows that $\hat{f}(u) \equiv f(u)$ if $f''(u) \ge 0$ on the interval $u_L \le u \le u_R$. $\hat{f}$ is always convex and has a nondecreasing derivative.

The solution to the Riemann problem at $\theta = \frac{x}{t}$ is defined as follows.

- **Case 1.** There exists a unique $u(\theta)$ such that $\hat{f}'(u(\theta)) = \theta$ and $\hat{f}''(u) > 0$ in a neighborhood of $u(\theta)$. In this case $u(\theta) = (\hat{f}')^{-1}(\theta)$. This point lies in a rarefaction fan.
- **Case 2.** $\hat{f}'(u)$ is constant over $a_L \le u \le a_R$ ($\hat{f}(u)$ is linear over $a_L \le u \le a_R$) and $\theta = \hat{f}'(a_L) = \hat{f}'(a_R)$. In this case, the resulting solution has a jump at θ: $u(\theta^-) = u_L$ and $u(\theta^+) = u_R$. This increasing jump in u corresponds to a contact discontinuity.
- **Case 3.** $\hat{f}'$ has an increasing jump at $u = u_0$ ($\hat{f}$ has a kink at $u = u_0$). Then

  $$u(\theta) = u_0, \text{ for } \hat{f}'(u_0^-) < \theta < \hat{f}'(u_0^+).$$

  This corresponds to a constant state.

We shall show that these three situations corresponds to three scenarios in Wulff crystal shape. The rarefaction wave corresponds to regions where the angle of the normal increases smoothly with the polar angle. The contact discontinuities correspond to the corner on a Wulff crystal where the angle of the normal jumps. The constant states correspond to the facets, where the normal to the Wulff shape points to a constant direction as the polar angle increases.

4.3. Geometric Construction of the Solution. The general conservation law (4.2) can formally be written as the convection equation $u_t + v(u)u_x = 0$, where the convective velocity is $v(u) = f'(u)$. The solutions to this can be visualized by letting each value u on the graph move horizontally with constant speed $v(u)$.

Based on this we obtain a simple geometric construction of the (possibly multiple-valued) solution to the Riemann problem. Each value from the initial step function u simply moves at its constant speed; in particular, each u value from the "step" itself, where u ranges between u_L to u_R at the single point $x = 0$, will propagate at its constant speed $v(u)$. Thus the resulting graph of u at any $t > 0$ will, when turned on its side, simply reproduce the graph of $v(u)$, u between u_L and u_R. This implies that $u(x,t)$ will be a multivalued solution of the Riemann problem if the graph of $v(u)$ is not monotone, i.e. if $v' = f''$ changes sign, as mentioned in the previous section.

To extract the physically correct single valued solution—the viscosity solution—we apply a geometric generalization of the conservation of the area under the graph of u implied by the original conservation law (4.2): At each overhang in the multiple-valued graph, introduce a jump that clips off the same amount overhanging area as it fills in on the underhang. Refer to figure 9.

The application of this clipping procedure to the multivalued solution at any time $t > 0$ will yield the proper single valued, time-self similar solution. Due to the self-similarity in time, the same shape results independent of t. Note the profile consists of constant regions to the far left and right, smooth regions where no clipping was necessary—"rarefactions"—and jumps where a clip was performed. These jumps in turn are classified as a "contact" if the velocity $v(u)$ is the same on each side of the jump, or a "shock" if the velocity causes u values one one side to overtake those on the other. Thus values appear to flow into a shock from both sides as time goes by.

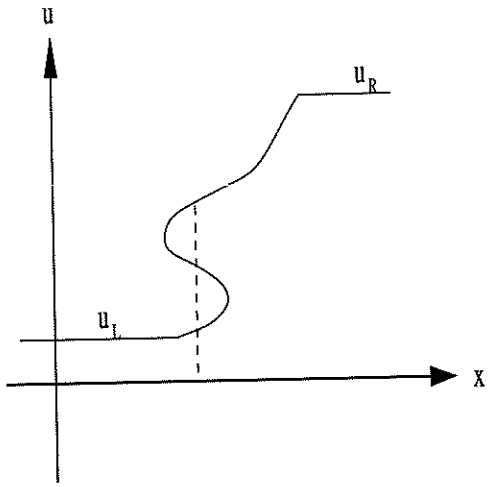

FIGURE 9. *The clipping procedure to the multivalued solution.*

While this clipping procedure is reasonable from the perspective of conserving u, it is not so easy to understand why it yields the true viscosity solution, i.e. the solution selected by the action of a small viscous dissipation.

5. The 2D Wulff Crystal as the Solution of a Riemann Problem

From the summaries of the Wulff Crystal and the Riemann problems, we can see a number of points of similarity in addition to the discontinuous nature of the solutions. Both problems admit self-similar solutions. Both are generally formulated in terms of integral equations. Both lead to governing differential equations that formally have multiple-valued "solutions". In both cases the multiple-valued solutions occur due to a lack of convexity, in the sense that a second derivative changes sign (in the Wulff problem its the sign of $\gamma + \gamma''$, in the Riemann problem, it is f''). And in both cases, there is a geometric construction that effectively truncates these multi valued solutions to yield the unique physical solution.

With this background in place, we are prepared to discuss the precise connection and differences between the two problems. There are several approaches that we can connect the Wulff shape with a Riemann problem of a scalar conservation law.

5.1. From the Euler-Lagrange Equation to a Scalar Conservation Law.

5.1.1. *The Basic Connection.* The first precise formal connection comes from rewriting the Euler-Lagrange equation (3.16) from Wulff's problem as the equation for the time self-similar solution of a Riemann problem 4.6. To do this, we define a function "flux function" $F(\nu)$ by the relation (assuming $\lambda = 1$)

$$F'' = \gamma + \gamma''. \tag{5.1}$$

Then the Euler-Lagrange equation (3.16) can be written as

$$(F'(\nu))_s = 1, \tag{5.2}$$

and integrating this yields

$$(F'(\nu(s))) - s = C, \tag{5.3}$$

where C is the constant of integration. By appropriate choice of the origin for the arclength parameter s, we can have $C = 0$. In this normalization, multiplying through by ν_s yields

$$(F'(\nu) - s)\nu_s = 0, \tag{5.4}$$

which is identical in form to the time self-similar equation (4.6). This in turn is the equation for the Riemann problem for the conservation law

$$\nu_t + (F(\nu))_x = 0. \tag{5.5}$$

Thus at least formally the normal angle $\nu(s)$ is the time self-similar solution to a Riemann problem for this conservation law. This would explain the crystal facets as constant states, the smooth faces as rarefactions, and the jumps in normal angle at crystal edges as shocks or contacts. However, this formal connection is not generally valid, because the differential equations used in the derivation only govern smooth solutions, i.e. crystal shapes with no edges and Riemann problems with no jumps. Whether a crystal shape with edges is the solution to this Ricmann problem must be investigated separately. It turns out that the conditions at jumps are different in the two problems, as described in the next subsection. Thus to completely realize the Wulff crystal as a Riemann problem solution requires a more subtle connection.

5.1.2. *Differences Between Wulff and Riemann Jump Conditions.* If the solution to a Riemann problem contains a propagating discontinuous jump, the differential equation for the conservation law (4.2) is not applicable at that point. However, the more general integral conservation law (4.1) still holds, and applied to a small interval containing the jump it yields the Rankine-Hugoniot jump condition

$$V(u^+ - u^-) = f(u^+) - f(u^-) \tag{5.6}$$

where V is the constant propagation speed of the discontinuity and u^+ and u^- are the right and left side values of u at the jump. This condition constrains the allowed jumps in a Riemann problem.

Similarly, if a Wulff crystal has a sharp edge with a jump in normal angle ν, the Euler-Lagrange equation (3.16) does not apply at that point. In this case, we can still identify a condition that governs the allowed jumps in angle. In the formal solution curve (3.17), the sharp corners on a crystal occur at points of self-intersection of the curve. These points separate the primary crystal shape from the artificial "swallowtail" shaped appendages that must be removed. Thus the jump condition at the edge is simply the condition for self intersection of this curve at two distinct normal angles ν_L and ν_R (corresponding to the normal direction on either side of the edge): $x(\nu_L) = x(\nu_R)$, or by the formula (3.17)

$$\gamma(\nu_L)\hat{n}(\nu_L) + \gamma'(\nu_L)\hat{\tau}(\nu_L) = \gamma(\nu_R)\hat{n}(\nu_R) + \gamma'(\nu_R)\hat{\tau}(\nu_R). \tag{5.7}$$

Taking the two components of this vector condition yields two scalar jump conditions.

If we compare the jump conditions for the specific Riemann problem (5.5) we formally associated with the Wulff crystal (i.e. $f = F$ from (5.1)), and the jump conditions (5.7) that hold for the true Wulff shape, it turns out they are different. The former has one constraint while the latter has two, and in addition, they allow different jumps. As we will see, the additional constraint comes from the fact that the allowed jumps is a contact discontinuity and must satisfy

$$f'(u_L) = f'(u_R) = \frac{f(u_R) - f(u_L)}{u_R - u_L}. \tag{5.8}$$

One can easily check that the flux F defined above does not possess this property at the corner.

This difference in jump conditions means that the discontinuous physical solutions to the Riemann problem (5.5) for $\nu(s)$ do not yield the correct normal angle function for Wulff shape. Thus for crystals with corners, a more careful construction is required to realize them as the solution to a Riemann problem.

The origin of this difference for discontinuous solutions can be traced back to the viscosity regularization used to define the unique solution of Riemann problem for conservation law (4.2). Evidently, this is *not* the proper regularization technique for use on the Euler-Lagrange differential equations for the Wulff problem. In retrospect this is not so surprising, since a proper regularizing correction for these equations should be derived by adding a physically reasonable energy penalty term to the original crystal energy (2.1), and using the variational calculus to derive the corresponding additional term in the Euler-Lagrange equations. The proper form of such a regularizing energy correction is considered in Gurtin's book [**11**].

5.1.3. *Reparameterization of Euler-Lagrange Equation.* In order to represent an arbitrary Wulff crystal as a solution to a related Riemann problem, we must take advantage of two additional degrees of freedom in the basic derivation. This added freedom will allow us to determine a flux for the Riemann problem such that the time self similar solution matching both the smooth parts and the jumps in the crystal shape.

The first freedom is that surface tension function γ can be replaced by an equivalent (i.e. resulting in the same Wulff shape) yet convex function $\hat{\gamma}$. This choice of $\hat{\gamma}$ will free us from considering self-intersection. But facets and jumps are still allowed.

The second degree of freedom is the choice of parameterization of the Wulff shape curve. So far we have used arc length, s, but if we used any other parameterization, $\alpha(s)$. the change of variables in the

Euler-Lagrange equation (3.16) would have the general form (using the equivalent $\hat{\gamma}$ instead of γ)

$$J(\hat{\gamma}(\nu)+\hat{\gamma}''(\nu))\nu_\alpha = 0, \tag{5.9}$$

where $J = \alpha_s$. If $J = J(\nu)$, we can follow the derivation of the basic Riemann problem from section 5.1.1 and conclude that the flux function $F(\nu)$ given by

$$F'' = J(\hat{\gamma}+\hat{\gamma}'') \tag{5.10}$$

defines a Riemann problem whose time self similar solutions match the smooth behavior of the Wulff shape $\nu(\alpha)$. The remaining freedom in choice of J can be used to match the proper jump conditions at the crystal shape corners.

In principle, this condition gives a set of equations defining the change of parameterization, J, and thus the flux F. In practice it would be tedious to blindly attempt to solve these equations. Fortunately, the proper reparameterization is one of the obvious possibilities, namely a change to standard polar coordinates for the Wulff shape curve. If we parameterize the normal direction at a point on the Wulff curve by the polar angle for that point, $\nu = \nu(\theta)$, we can show by using chain rule that

$$\theta_s = \frac{\hat{\gamma}}{(\hat{\gamma}')^2+\hat{\gamma}^2}. \tag{5.11}$$

The corresponding flux function from (5.10) is then defined by

$$F'' = \frac{\hat{\gamma}(\hat{\gamma}+\hat{\gamma}'')}{\hat{\gamma}^2+\hat{\gamma}'^2}. \tag{5.12}$$

This can be integrated to obtain an explicit formula for the flux function,

$$F(\nu) = \frac{1}{2}\nu^2 + \int_0^\nu \tan^{-1}\left(\frac{\hat{\gamma}'(u)}{\hat{\gamma}(u)}\right) du. \tag{5.13}$$

The time self similar viscosity solution to the appropriate Riemann problem for the corresponding hyperbolic conservation law $\nu_t + F(\nu)_\xi = 0$ is exactly the Wulff shape parameterized as $\nu(\theta)$.

We now verify by directly checking that the contact jump conditions (5.8) agree with the Wulff jump conditions (5.7) in this case. Suppose ν jumps from ν_L to ν_R. Then from the discussion in section 4.2, $\hat{\gamma}(\nu)+\hat{\gamma}''(\nu) \equiv 0$ for $\nu_L \le \nu \le \nu_R$ and F is linear over this interval. Note that

$$\theta = F'(\nu) = \nu + \tan^{-1}\left(\frac{\hat{\gamma}'(\nu)}{\hat{\gamma}(\nu)}\right).$$

So the first equality in contact jump condition (5.8) means

$$\theta_L = \theta_R.$$

The conclusion follows from (3.24) in section 3.4.

In retrospect, the correct form of flux is also the most natural one if we write the corresponding conservation law as

$$\frac{\partial \nu}{\partial t} + F'(\nu)\frac{\partial \nu}{\partial \xi} = 0 \tag{5.14}$$

whose characteristic equations are

$$\begin{cases} \frac{d\xi}{dt} = \theta(\nu), \\ \frac{d\nu}{dt} = 0, \end{cases} \tag{5.15}$$

which simply say that ν is constant along the ray emanating from the origin with polar angle $\theta = \xi/t$. This is obviously true for the self-similar growth of Wulff crystal shape.

5.2. Self-Similar Growth of Wulff Shape and Riemann Problem. In section 2.3, we have seen that Wulff shape growing with the normal velocity equal to its surface tension is a simple self-similar dilation. We now try to find the evolution equation that governs the normal angle. We assume γ is convex in this section. Otherwise just replace γ with its Frank convexification $\hat{\gamma}$.

To start with, choose the x-axis so that it intersects with Wulff shape at a minima of the surface energy. From Wulff's construction, the normal at this point and the x-axis coincide. Since the growth is self similar, this point will remain on the x-axis. As before, let ν be the normal angle to the positive x-axis. and s the arclength parameter. In Appendix II, we derive the evolution equation of ν to be

$$\frac{\partial \nu}{\partial t} + \int_0^{\nu} [\gamma(u) + \gamma''(u)]\, du \frac{\partial \nu}{\partial s} = 0. \tag{5.16}$$

If we let $F''(\nu) = \gamma(\nu) + \gamma''(\nu)$, then the above equation becomes

$$\frac{\partial \nu}{\partial t} + \frac{F(\nu)}{\partial s} = 0. \tag{5.17}$$

This is the same as (5.5) which we derived above.

Note that using the arclength s as a parameter is not a good choice, because for a self similar growth, the point on the interface that moves on a straight line away from the origin corresponds to different values of s at different time. This issue actually predicts a problem with this connection. As we have seen before, the above conservation law does not give the right solution.

The correct equation can be obtained by a change of variables in the equation (5.17) which governs the evolution of the angle of the normal. We introduce the following new set of variables:

$$\begin{cases} \tau = t, \\ \xi = t\theta(t, s) \end{cases} \tag{5.18}$$

where $\theta(t, s)$ is defined implicitly by:

$$\frac{s}{t} = \int_0^{\nu(\theta)} [\gamma(\nu) + \gamma''(\nu)]\, d\nu \tag{5.19}$$

and $\nu(\theta)$ in turn is defined by

$$\theta = \nu + \tan^{-1}\left(\frac{\gamma'(\nu)}{\gamma(\nu)}\right).$$

The equation under this new set of variables is

$$\frac{\partial \nu}{\partial \tau} + \frac{\partial F(\nu)}{\partial \xi} = 0, \tag{5.20}$$

where $F(\nu) = \frac{1}{2}\nu^2 + \int_0^{\nu} \tan^{-1}\left(\frac{\gamma'(u)}{\gamma(u)}\right) du$. This coincides with (5.13) above. See Appendix II for the derivation.

5.3. Main Theorem and Its Consequences. We have at least formally demonstrated through two quite different approaches that the Wulff shape is connected with the Riemann problem for a scalar conservation law. This is the major result of this paper. We summarize it in the following theorem and explore some of its consequences.

THEOREM 5.1. *Let $\gamma : S^1 \to R^+$ be continuous and let its Frank convexification $\hat{\gamma}$ be piecewise differentiable. Let W be the Wulff shape corresponding to surface tension γ, as defined by Wulff's construction, and $\nu(\theta)$ be the angle of the outward normal to W as a function of polar angle θ, in the polar coordinate system with origin at the centroid of W, and the horizontal axis passes through a global minima of the surface tension. Then for all θ where $\nu(\theta)$ is well-defined and differentiable*

$$\nu(\theta) = -\frac{d}{d\theta} \min_{0 \le \nu \le 2\pi} [F(\nu) - \theta\nu], \tag{5.21}$$

where F is the function on $[0, 2\pi]$ defined by

$$F(\nu) = \frac{\nu^2}{2} + \int_0^{\nu} \tan^{-1}\left(\frac{\hat{\gamma}'(\alpha)}{\hat{\gamma}(\alpha)}\right) d\alpha. \tag{5.22}$$

Furthermore, $\nu(\xi,t) \equiv \nu(\frac{\xi}{t})$ *is the time self-similar viscosity solution to the Riemann problem*

$$\nu_t + (F(\nu))_\xi = 0, \tag{5.23}$$

$$\nu(\xi < 0, t = 0) = 0, \tag{5.24}$$

$$\nu(\xi > 0, t = 0) = 2\pi. \tag{5.25}$$

The proof follows from Theorem 3.3 and Osher's formula (4.7) for the Riemann problem for a scalar conservation law.

This theorem serves as a bridge that connect the world of gas dynamics, which has a long history and has been extensively studied (See the book by Courant and Friedrich [6]) with the fascinating world of crystal shapes which is characterized by facets, edges and corners. We can characterize these shapes in term of the flux F, which is a convex function. The facet corresponds to a kink in the graph of F in R^2, which in turn corresponds to constant states in the world of gas dynamics; The corner corresponds to a piece of a straight line in the graph of F, which in the world of gas dynamics corresponds to contact jumps; We observe rounded edges when a crystal melts, and the sharp corners become smooth out. These regions correspond to the smooth region in the graph of F, and, in the conservation law analogue, they correspond to rarefaction waves.

We can also characterize these phenomena with the polar plot of $\hat{\gamma}$. Here the facets correspond to cusps, and the corners correspond to circular arcs in the polar plot of $\hat{\gamma}$.

Conceptually, we have fully clarified the initial intuitive similarity between these disparate problems: at least in 2D, it is completely accurate to say that the corners on a crystal are contact discontinuities, the smooth faces are rarefactions, the facets are constant states, for a generally discontinuous solution of a hyperbolic conservation law.

5.4. A Convex Example. We consider the surface tension

$$\gamma(\nu) = |\cos(\nu)| + |\sin(\nu)|. \tag{5.26}$$

This is an important example, since this surface tension arises in the continuum limit of the simple X-Y lattice model of a crystal. However, it is also quite simple to analyze. We will also remark on how it relates to the general case where appropriate.

Note that the key measure of convexity, $\gamma + \gamma''$, vanishes almost everywhere, but does not change sign. In fact, as a distribution it is

$$\gamma(\nu) + \gamma''(\nu) = \sum_{k=0}^{3} \delta(\nu - k\frac{\pi}{2}) \tag{5.27}$$

$$\geq 0. \tag{5.28}$$

Because this quantity appears in the Euler-Lagrange equation (3.16) and in the generalized solution (3.17), these are both degenerate. The solution curve $x(\nu) = \gamma(\nu)\hat{n}(\nu) + \gamma'(\nu)\hat{\tau}(\nu)$ is readily computed, and its image consist of just four isolated points, shown in figure 10 (c),

$$x(\nu) = \begin{cases} (+1,+1), & 0 < \nu < \frac{\pi}{2}. \\ (-1,+1), & 0 < \nu < \pi. \\ (-1,-1), & 0 < \nu < \frac{3\pi}{2}. \\ (+1,-1), & 0 < \nu < 2\pi. \end{cases} \tag{5.29}$$

Connecting these dots into a continuous curve yields a square, which is the Wulff shape. Note that in this example, no multivalued swallowtails occur because there is no sign change in $\gamma + \gamma''$. Also, the image curve consists only of isolated vertices, since, by equation (3.18), the tangent vector x' is proportional to $\gamma + \gamma''$ and thus vanishes almost everywhere.

Wulff's geometric construction also leads to the same shape. The surface tension polar plot is the "four leaf clover" shown in figure 10 (a), consisting of four symmetrically positioned arcs of circles that, if extended, would pass through the origin. Wulff's geometric construction places one facet at each cusp in the polar plot, and together these form a square as shown in figure 10 (d). The virtual facets placed at all other points along the polar plot lie entirely outside this square, and so the inner envelope defining the Wulff shape is the square itself. The simplicity of the the construction is due to the fact that the polar plot is composed

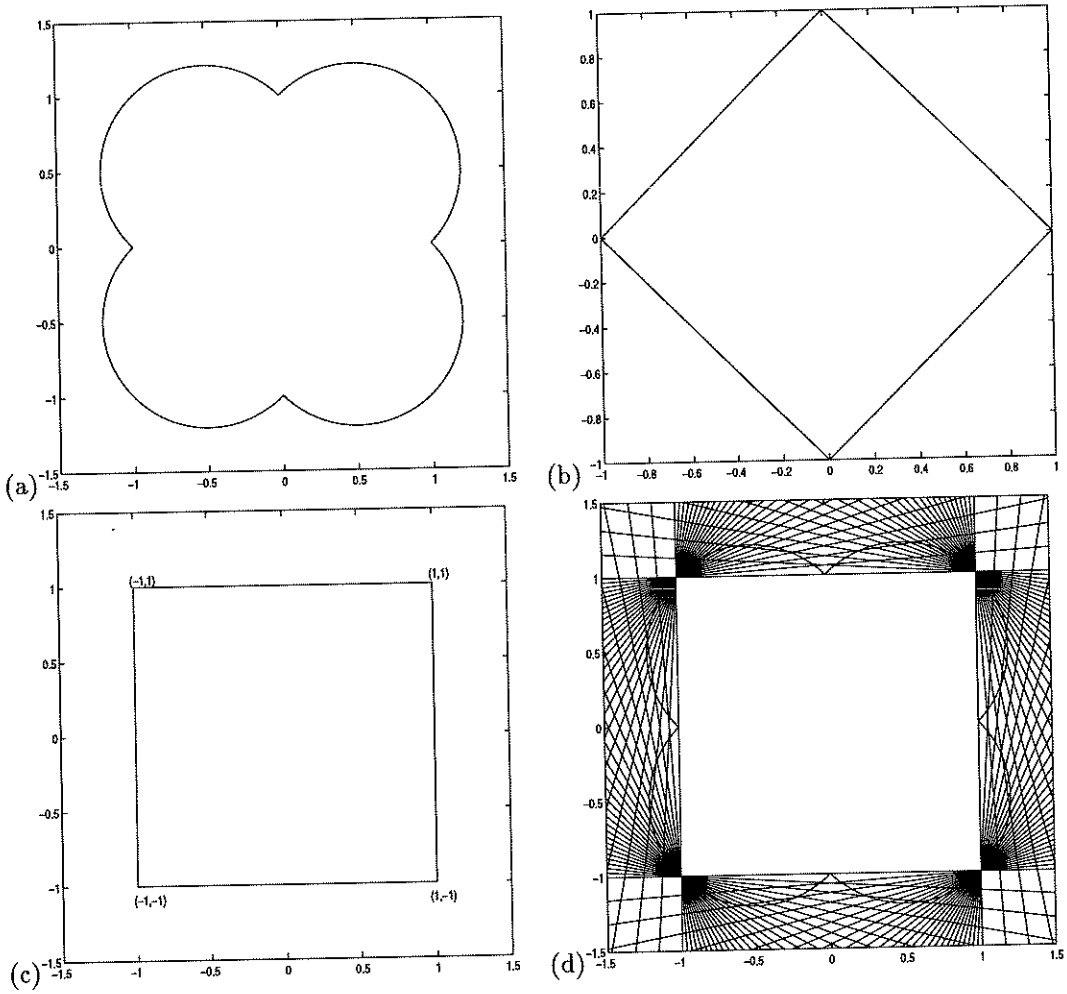

FIGURE 10. *(a) Plot of surface tension γ. (b) Plot of $\frac{1}{\gamma}$. (c) Plot of $\gamma(\nu)\hat{n}(\nu)+\gamma'(\nu)\hat{\tau}(\nu)$. (d) Crystal shape from Wulff's geometric construction.*

of circular arcs; these are always "dual" to a single vertex in a polygonal Wulff shape (refer to [**10**] for the general properties of this duality).

Next we consider the details of the Riemann problem construction. The first step is to compute the flux function (5.13). Recall the that the flux function is based on the Frank convexified surface tension, $\hat{\gamma}$. However, the surface tension function in this example is already "convex", in the appropriate sense, i.e. $\gamma+\gamma'' \geq 0$. Thus $\hat{\gamma}=\gamma$, and this is a major source of simplification over the general surface tension case. Note that in general the Frank convexified surface tension will replace any nonconvex portion of the polar plot (i.e. segment where $\gamma+\gamma'' < 0$ with the arc of a circle passing through the origin, since that is the curve of neutral convexity (i.e. with $\gamma+\gamma''=0$. Because of this, the surface tension used in this example is representative of what generally occurs after convexification.

To compute the flux function, it greatly simplifies the trigonometry to note that

$$\gamma(\nu)=\sqrt{2}\cos(\nu-\phi(\nu)) \tag{5.30}$$

where the phase shift $\phi(\nu)$ is

$$\phi(\nu)=\frac{\pi}{4}(2k-1),(k-1)\frac{\pi}{2}<\nu<k\frac{\pi}{2}, \tag{5.31}$$

or, more succinctly,

$$\phi(\nu)=\frac{\pi}{4}(2[\frac{\nu}{\pi/2}]-1), \tag{5.32}$$

where $[x]$ denotes the least integer $\geq x$.

From this we get that

$$\frac{\gamma'}{\gamma} = \tan(-\nu + \phi(\nu)), \tag{5.33}$$

or,

$$\tan^{-1}(\frac{\gamma'}{\gamma}) = -\nu + \phi(\nu). \tag{5.34}$$

Applying this in the flux formula 5.13, we get

$$F(\nu) = \frac{\nu^2}{2} + \int_0^\nu -y + \phi(y)dy \tag{5.35}$$

$$= \int_0^\nu \phi(y)dy \tag{5.36}$$

$$= \frac{\pi}{4}([u]^2 + (1 - 2[u])([u] - u)), \tag{5.37}$$

where $u = \frac{\nu}{\pi/2}$. The graph of F is shown in figure 11. F can easily described by noting that it is a piecewise linear function that linearly interpolates the values $F(k\frac{\pi}{2}) = \frac{\pi}{4}k^2$, for integers $k = 0, 1, 2, \ldots$. These values in turn lie on the parabola $f(\nu) = \nu^2/\pi$. Note that the linear segment of the graph beginning at $\nu = k\frac{\pi}{2}$ has slope $(2k+1)\frac{\pi}{4}$. Considering the relation to the general surface tension case, note that the piecewise linear segments of the graph of the flux correspond to portions of the polar plot where $\hat{\gamma} + \hat{\gamma}'' = 0$ (or, geometrically, the surface tension polar plot is a circular arc), and that these will be present wherever the surface tension required convexification. Thus they will be a typical feature of the general case.

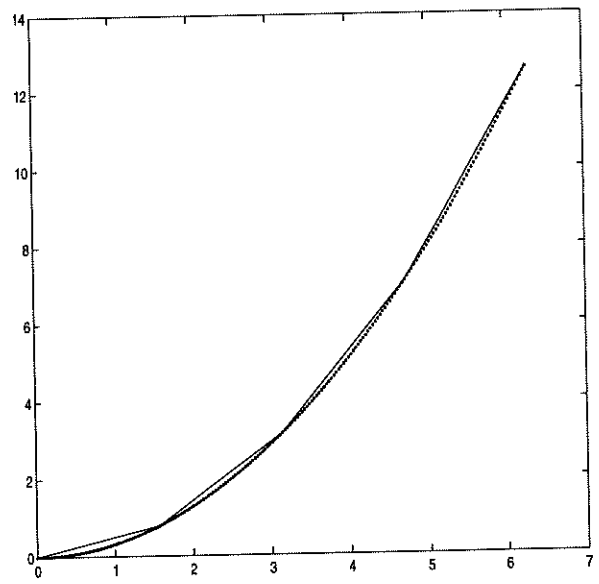

FIGURE 11. *The flux function (the solid line). The dashed line is the graph of* ν^2/π.

With the flux F in hand, we can now work out the analytic form of the Riemann problem solution from formula (5.21). The first step is to find, for a given θ in $[0, 2\pi]$, the minimal value of $F(\nu) - \theta\nu$. Note this function is also a piecewise linear (in ν) function inscribed in a parabola, and so its minimum will be at the vertex where its slope switches from negative to positive as indicated in figure 11. This in turn will occur where $F(\nu)$ changes from having slope less that θ to slope greater than θ. Call this point $\nu_{\min}(\theta)$. It can be described precisely as follows: if θ lies between $\theta_1 = (2k-1)\frac{\pi}{4}$ and $\theta_2 = (2k+1)\frac{\pi}{4}$, then the transition in the slope of F will occur at $\nu_{\min}(\theta) = (k-1)\frac{\pi}{2}$, at which point the slope changes from θ_1 to θ_2. Note that

for a given θ, k is simply the *nearest integer* to $\frac{\theta}{\pi/2}$. Thus we can write

$$\nu_{\min}(\theta) = (N(\frac{\theta}{\pi/2}) - 1)\frac{\pi}{2}, \tag{5.38}$$

where $N(x)$ is the nearest integer to x. In particular, the minimizing argument is a piecewise constant function of θ.

Continuing to unravel the Riemann problem solution formula (5.21), we see that for θ in an interval for which the minimizing argument $\nu_{\min}(\theta)$ remains *constant* with value ν_{min}, we have

$$\min_{0\le\nu\le 2\pi}(F(\nu) - \theta\nu) = F(\nu_{min}) - \theta\nu_{min} \tag{5.39}$$

and thus the solution to the Riemann problem for that range of θ is

$$\nu(\theta) = -\frac{d}{d\theta}\min_{0\le\nu\le 2\pi}(F(\nu) - \theta\nu) \tag{5.40}$$

$$= -\frac{d}{d\theta}(F(\nu_{min}) - \theta\nu_{min}) \tag{5.41}$$

$$= \nu_{min}. \tag{5.42}$$

Applying this over the respective θ intervals corresponding to $\nu_{min} = 0, \pi/2, \pi, 3\pi/2$, we obtain the complete Riemann problem solution as

$$\nu(\theta) = \begin{cases} 0, & 0 \le \theta < \pi/4. \\ \pi/2, & \pi/4 < \theta < 3\pi/4. \\ \pi, & 3\pi/4 < \theta < 5\pi/4. \\ 3\pi/2, & 5\pi/4 < \theta < 7\pi/4. \\ 2\pi, & 7\pi/4 < \theta \le 2\pi. \end{cases} \tag{5.43}$$

This is precisely the angle of the normal vector (to the x-axis) as a function of polar angle θ for a square shape centered at the origin. Thus the solution to the Riemann problem describes the square Wulff shape.

Finally, we can also recover the Wulff shape via the geometric solution to the Riemann problem. For this, we first graph the initial data for $\nu(\xi, t)$, which has left and right states 0 and 2π with the jump at $\xi = 0$. Then we graph $v(\nu) = F'(\nu)$ along the ν axis. In this case, $v(\nu)$ is the piecewise constant function with values $(2k+1)\pi/4$ over the ν intervals $(k\pi/2, (k+1)\pi/2)$, for $k = 0, 1, 2, 3$. Because of the convexity of the flux $F(\nu)$, there are no overhangs in the resulting plot, i.e. it defines a single valued function of $\nu(\xi)$ over the ξ axis. This function is the self-similar solution, $\nu(x, t) = \nu(x/t)$. We see as before that $\nu(\theta)$ is the same function found via the analytic solution to the Riemann problem, and thus it again describes the square Wulff shape. Regarding the general case, note that the flux will always be convex, since $F'' = \frac{\hat{\gamma}(\hat{\gamma}+\hat{\gamma}'')}{\hat{\gamma}^2+\hat{\gamma}'^2} \ge 0$. Thus in this geometric construction, the graph of $v(\nu)$ will always result in a single valued $\nu(\xi)$, and there will be no need for the equal area procedure of clipping off multivalued overhangs as described in the general geometric algorithm for solving the Riemann problem.

5.5. A Nonconvex Example. Now let us consider the following surface tension

$$\gamma(\nu) = 1 + |\sin(2\nu)|. \tag{5.44}$$

The Wulff shape of this γ is also a square. See figure 12 (d). This surface tension is nonconvex, since

$$\gamma(\nu) + \gamma''(\nu) = \begin{cases} 1 - 3\sin(2\nu), & \text{for } \nu \in [0, \frac{\pi}{2}] \cup [\pi, \frac{3\pi}{2}]. \\ 1 + 3\sin(2\nu), & \text{for } \nu \in [\frac{\pi}{2}, \pi] \cup [\frac{3\pi}{2}, 2\pi]. \end{cases} \tag{5.45}$$

changes sign as ν goes from 0 to 2π. It turn out that its Frank convexification $\hat{\gamma}(\nu) = |\cos\nu| + |\sin(\nu)|$, which is exactly the surface tension that we discussed in the section above. Replace γ by $\hat{\gamma}$, we are back to the example in the last section. Refer to figure 12.

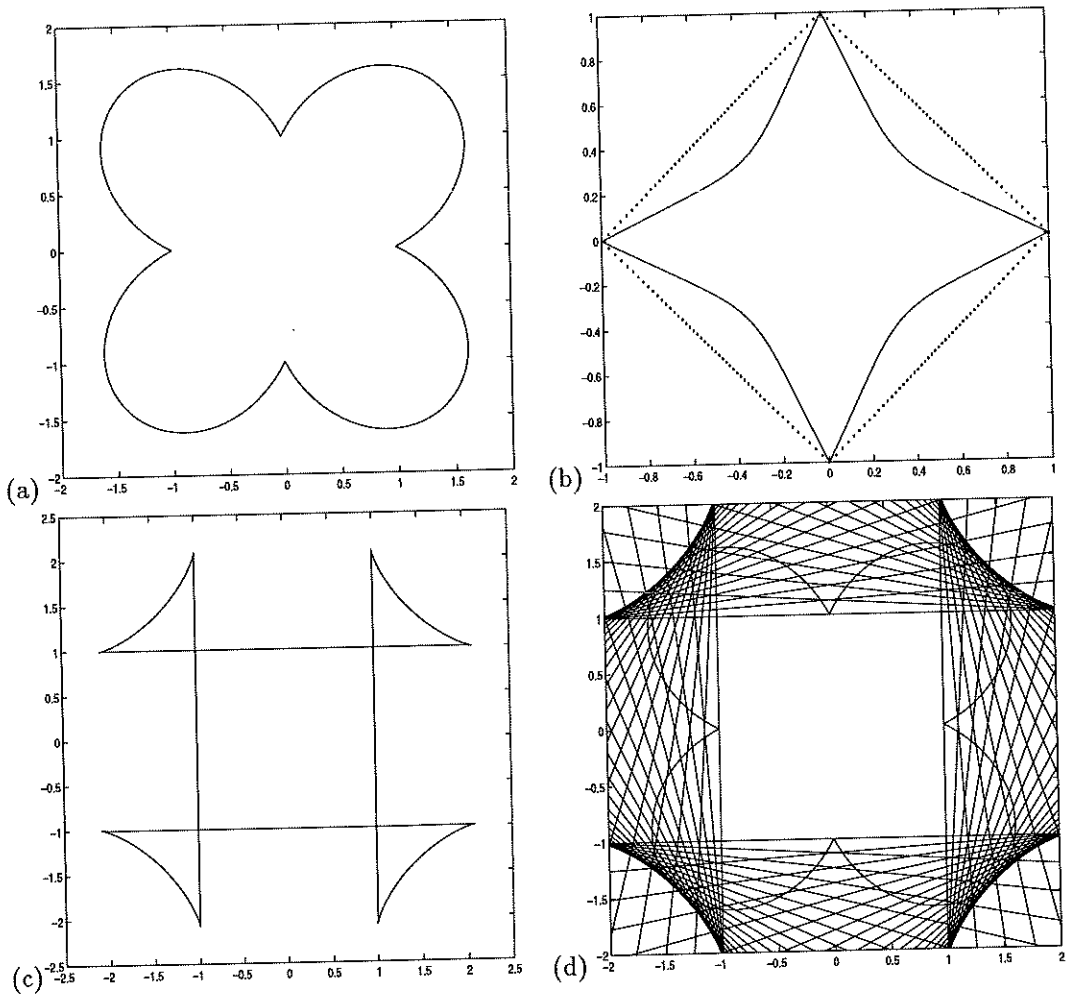

FIGURE 12. *(a) Plot of surface tension γ. (b) The solid line is the plot of $\frac{1}{\gamma}$, and the dashed line is the plot of $\frac{1}{\tilde{\gamma}}$. (c) Plot of $\gamma(\nu)\hat{n}(\nu)+\gamma'(\nu)\hat{\tau}(\nu)$. The self-intersection of the plot indicates that this γ is nonconvex. (d) The Wulff crystal shape from Wulff's geometric construction.*

6. Some Comments on The Wulff Problem in Higher Dimensions

We have seen in section 2.3 that the growth of Wulff crystal shape with its (convexified) surface energy is simply a self-similar dilation. Suppose we grow a crystal from a infinitesimal initial Wulff shape, and at time $t = 1$ the Wulff shape is given by $W(\theta) = \gamma_*(\theta)$, then the unit outwards normal at a certain later time satisfies

$$\hat{n}(t, t\mathbf{W}(\theta)) = \hat{n}(1, \mathbf{W}(\theta)).$$

Denote $t\mathbf{W}(\theta)$ as ξ, and differentiate with respect to t, we get

$$\hat{n}_t + \mathbf{W}(\theta) \cdot \nabla_\xi \hat{n} = 0, \tag{6.1}$$

where $\nabla_\xi \hat{n}$ is the gradient of $\hat{n}$. Recall that $\mathbf{W}(\theta) = D\gamma(\hat{n})$, we get the following

$$\frac{\partial \hat{n}}{\partial t} + \sum_{k=1}^{n} \frac{\partial \gamma}{\partial n_k}(\hat{n}) \frac{\partial \hat{n}}{\partial \xi_k} = 0. \tag{6.2}$$

This is a system of hyperbolic equations. The question of whether this system can be transformed into a system of conservation laws through a choice of suitable variables is still open.

At present, the relation between 3D Wulff shapes and nonlinear wave dynamics is unclear. However, the original intuitive connection between crystals and shock waves remains compelling in 3D, and the possibility of some such relation calls for further investigation.

7. The Level Set Formulation for the Wulff Problem

The level set method of Osher and Sethian [17] has been very succcssful as a computational tool in capturing the moving interfaces, especially when the interface undergoes topological changes. It is also useful for the theoretical analysis of the variational problem associated with Wulff crystals. We now briefly review this method and apply it to the Wulff problem.

7.1. The Level Set Representation of Surface Energy. Suppose Ω is a open region in R^d which may be multi-connected. Let $\Gamma = \partial\Omega$ be its boundary. We define an auxiliary function ϕ so that

$$\begin{cases} \phi(x) < 0, \text{ if } x \in \Omega. \\ \phi(x) = 0, \text{ if } x \in \Gamma. \\ \phi(x) > 0, \text{ otherwise.} \end{cases} \tag{7.1}$$

For example, we can choose ϕ to be the signed distance function to the interface Γ. Indeed, for computational accuracy, this is the most desirable case. We call ϕ the level set function of Γ.

Many geometric quantities have simple expressions in terms of level set function. For example, the outward unit normal direction $\hat{n} = \frac{\nabla\phi}{|\nabla\phi|}$, the mean curvature $\kappa = \nabla \cdot \frac{\nabla\phi}{|\nabla\phi|}$, and the area element (or arclength element) $dA = \delta(\phi)|\nabla\phi|dx$. The surface energy over Γ can be expressed as

$$E(\phi) = \int \gamma(\frac{\nabla\phi}{|\nabla\phi|})\delta(\phi)|\nabla\phi|dx \tag{7.2}$$

where δ is the 1 dimensional δ function.

7.2. The Euler-Lagrange Equation for the Wulff Problem. Once we write the surface energy in terms of the level set function, the Wulff problem becomes to find the particular level set function that minimizes the surface energy subject to the constraint that its zero contour enclosed a fixed volume. We extend γ to the whole space as a homogeneous function of degree 1(which we still denote as γ) and introduce a Lagrange multiplier λ. The Lagrangian is:

$$\mathcal{L}(\phi, \lambda) = \int \gamma\left(\frac{\nabla\phi}{|\nabla\phi|}\right)\delta(\phi)|\nabla\phi|dx - \lambda\int H(-\phi)dx, \tag{7.3}$$

where $H(\phi)$ is the Heaviside function which is 0 for $\phi < 0$ and 1 otherwise.

In Appendix III, we show that the Euler-Lagrange equation for (7.3) is

$$\sum_{j=1}^{n}\frac{\partial}{\partial x_j}\left[\frac{\partial\gamma}{\partial p_j}(\frac{\nabla\phi}{|\nabla\phi|})\right] = \lambda, \tag{7.4}$$

or in a more compact form

$$\nabla \cdot \left[D\gamma(\frac{\nabla\phi}{|\nabla\phi|})\right] = \lambda, \tag{7.5}$$

where the constant λ is chosen so that the volume is as given.

Note the denominator in the above expression is simply the perimeter (in 2D) or area (in 3D) of Γ. In 2D, equation (7.4) becomes the familiar formula (3.16).

The gradient flow of the Wulff energy is

$$\phi_t = |\nabla\phi|\left[\nabla D\gamma\left(\frac{\nabla\phi}{|\nabla\phi|}\right) - \lambda\right], \tag{7.6}$$

where λ is given by

$$\lambda = \frac{\int \nabla \cdot \left[D\gamma(\frac{\nabla\phi}{|\nabla\phi|})\right]\delta(\phi)|\nabla\phi|dx}{\int \delta(\phi)|\nabla\phi|dx}, \tag{7.7}$$

so that the area is fixed and the energy is decreasing under the gradient flow.

Equation (7.6) is fully nonlinear weakly parabolic type equation when γ is convex in the sense defined in section 2.3, and is of mixed type when γ is not. How to regularize the variational problem by adding an appropriate penalty term is an interesting question. We shall discuss this issue in future work. See Gurtin's book [**11**] for some discussions of this matter.

7.3. The Hamilton-Jacobi Equation for a Growing Wulff Crystal. Now let the interface move with normal velocity equal to V, which might depend on some local and global properties of the interface Γ. Denote the boundary at a later time t as $\Gamma(t)$, and the associated level set function as $\phi(t,x)$. Let $x(t)$ be a particle trajectory on the interface. By definition, $\phi(t,x(t)) = 0$. By differentiating with respect to t, and noting that $V = \dot{x}(t) \cdot \frac{\nabla\phi(x)}{|\nabla\phi(x)|}$, we get

$$\phi_t + V|\nabla\phi| = 0. \tag{7.8}$$

This is a Hamilton-Jacobi equation if V depends only on x, t, and $\nabla\phi$. The location of the interface is find by solving this equation and then finding its zero level set $\{x : \phi(t,x) = 0\}$. Thus a vast wealth of recent extensive theoretical and numerical research on Hamilton-Jacobi equations can be applied to the moving interface problem.

It was shown in [**19**] that Wulff shape growing with normal velocity equal to surface tension is a self-similar dilation. For any other shape (which may be multiply connected), one can place two concentric Wulff shapes, such that one is contained by this shape, and the other contains this shape, and then let them grow with surface tension. Since the arbitrary shape will always be confined between the two Wulff shapes by the comparison principle for the viscosity solutions to Hamilton-Jacobi equations, one immediately concludes that the asymptotic shape growing from any initial configuration is a Wulff crystal shape. For details of the proof with error bounds, see the recent paper [**19**] by Osher and Merriman. This approach give us a very convenient way to find the Wulff shape numerically for a given surface energy, especially in 3D. The next section contains many examples demonstrating this.

By embedding the interface problem into a one dimensional higher space, it appears that a substantial increase in computation cost is incurred. This is not true, because we are only interested in the behavior of the zero level set. A localized method can be used to lower the computational expense. This is discussed in [**1, 25**] and a more recent paper [**20**]. The method in [**20**] is the one that we used in our numerical examples below.

8. Numerical Examples

We present in this section some numerical results obtained by solving equation (7.8) with $V = \frac{\nabla\phi}{|\nabla\phi|}$, that is,

$$\phi_t + \gamma(\frac{\nabla\phi}{|\nabla\phi|})|\nabla\phi| = 0, \quad x \in R^d, t > 0 \tag{8.1}$$

with a fast localized level set method coupled with a PDE based re-initialization step developed in [**20**] using the ENO [**18**] or WENO [**14**] schemes for Hamilton-Jacobian equations.

First, let us briefly review the numerical schemes that we shall use below for a general Hamilton-Jacobi equation:

$$\phi_t + H(\nabla\phi) = 0, \qquad x \in R^d, t > 0. \tag{8.2}$$

To simplify notation, we will only write down the formulae for the 2D case. The extension to higher dimensions is straightforward.

The semi-discrete version of (8.2) in 2D is:

$$\frac{\partial\phi_{ij}}{\partial t} = -\hat{H}(\phi^+_{x,ij}, \phi^-_{x,ij}, \phi^+_{y,ij}, \phi^-_{y,ij}), \tag{8.3}$$

where $\phi^\pm_{x,ij}$ and $\phi^\pm_{y,ij}$ are one-sided approximations to the partial derivatives ϕ_x and ϕ_y at (x_i, y_j), respectively. $\hat{H}$ is a numerical Hamiltonian that is monotone and consistent with H. See [**8**] or [**18**] for more details.

In our computations, $\phi^{\pm}_{x,ij}$ and $\phi^{\pm}_{y,ij}$ are calculated with the 3rd order ENO scheme of Osher and Shu [18] or the 5th order WENO scheme of Jiang and Peng [14] for Hamilton-Jacobi equations, and $\hat{H}$ is chosen as the following Lax-Friedrichs (LF) flux:

$$\hat{H}^{LF}(u^+,u^-,v^+,v^-) = H(\frac{u^+ + u^-}{2}, \frac{v^+ + v^-}{2}) - \frac{\alpha}{2}(u^+ - u^-) - \frac{\beta}{2}(v^+ - v^-) \tag{8.4}$$

where α and β are artificial viscosities defined by:

$$\alpha = \max_{\substack{u\in[A,B]\\ v\in[C,D]}} |H_1(u,v)|, \qquad \beta = \max_{\substack{u\in[A,B]\\ v\in[C,D]}} |H_2(u,v)|. \tag{8.5}$$

Here $H_1 = \partial H/\partial u$, $H_2 = \partial H/\partial v$, $[A,B]$ and $[C,D]$ are the range of $u^{\pm}$ and $v^{\pm}$, respectively.

Solutions to (8.1) often will become either too flat or too steep near the interface $\{\phi = 0\}$ even if the initial data is a perfect signed distance function. In order to avoid numerical difficulties and retain accuracy, an additional operation, which is called re-initialization, is needed to reset ϕ to be a distance function again. This becomes essential for the localized level set method of [20]. In [26], a PDE based re-initialization method was proposed. By solving the following equation:

$$\begin{cases} \phi_t + sign(\phi_0)(|\nabla\phi| - 1) = 0 \quad \text{in } R^d \times R_+, \\ \phi(x,0) = \phi_0(x) \end{cases} \tag{8.6}$$

to steady state, the original level set function ϕ_0 becomes a distance function to the front defined by $\{\phi_0 = 0\}$. For (8.6), we use the Godunov numerical Hamiltonian:

$$H^{God}(u^+,u^-,v^+,v^-) = \begin{cases} s\sqrt{[\max((u^+)^-,(u^-)^+)]^2 + [\max((v^+)^-,(v^-)^+)]^2}, & \text{if } \phi^0_{ij} \geq 0. \\ s\sqrt{[\max((u^+)^+,(u^-)^-)]^2 + [\max((v^+)^+,(v^-)^-)]^2}, & \text{otherwise.} \end{cases} \tag{8.7}$$

where $\phi^0_{ij} = \phi_0(x_i,y_j)$, $(a)^+ = \max(a,0)$,$(a)^- = \max(-a,0)$, and $s = \phi_0/\sqrt{\phi_0^2 + \Delta x}$ is an approximation to $sign(\phi_0)$.

For the time discretization, we use the 3rd order TVD Runge-Kutta scheme developed in [23]. Consider the following ODE:

$$\frac{d\phi}{dt} = L(\phi), \qquad \phi(0) = \phi_0. \tag{8.8}$$

The 3^{rd} order TVD Runge-Kutta method at the n^{th} step is:

$$\begin{aligned} \phi^{(1)} &= \phi^n + \Delta t L(\phi^n), \\ \phi^{(\frac{1}{2})} &= \phi^n + \frac{\Delta t}{4}\{L(\phi^n) + L(\phi^{(1)})\}, \\ \phi^{n+1} &= \phi^n + \frac{\Delta t}{6}\{L(\phi^n) + 4L\phi^{(\frac{1}{2})} + L(\phi^{(1)})\}. \end{aligned} \tag{8.9}$$

In all the examples below except for the first one, the computation is performed in the region $[-1,1]^2$ in 2D, and $[-1,1]^3$ in 3D. The time step Δt is chosen as $.1\Delta x$, and for the re-initialization step it is $.5\Delta x$. Since the computation is only done near the front in both the approximation to (8.1) and (8.6), we observe a considerable speed up of approximately 7 times over the global method. In example 2, 3, 4 and 5, we start from a circle or sphere purely for simplicity in preparing the initial data. It is interesting to see initial objects merge and asymptote to the Wulff shape. This is displayed in figure 28 in example 6, where we start from amultiply connected initial shape.

Example 1. To test our main result Theorem 5.1 in section 5.3, we solve the scalar conservation law (5.23)—(5.25) directly with the 3rd order ENO scheme for conservation laws developed in [24] by Shu and Osher , for the case $\gamma(\nu) = |\cos\nu| + |\sin\nu|$. We have found the flux function $F(\nu)$ for this problem in section 5.4. See figure 13.

Example 2. (2D) We start from a circle and evolve it with normal velocity equal to $\gamma(\nu)$, where ν is the angle between the outward normal direction $\hat{n} = \frac{\nabla\phi}{|\nabla\phi|}$ and the x-axis, $-\pi \leq \nu \leq \pi$. We use a 200×200 grid. The pictures in figure 14–22 on the left are the crystalline shapes obtained from Wulff's construction, the corresponding pictures on the right are the shapes obtained from evolution. We print out the evolving shapes every 50 time steps.

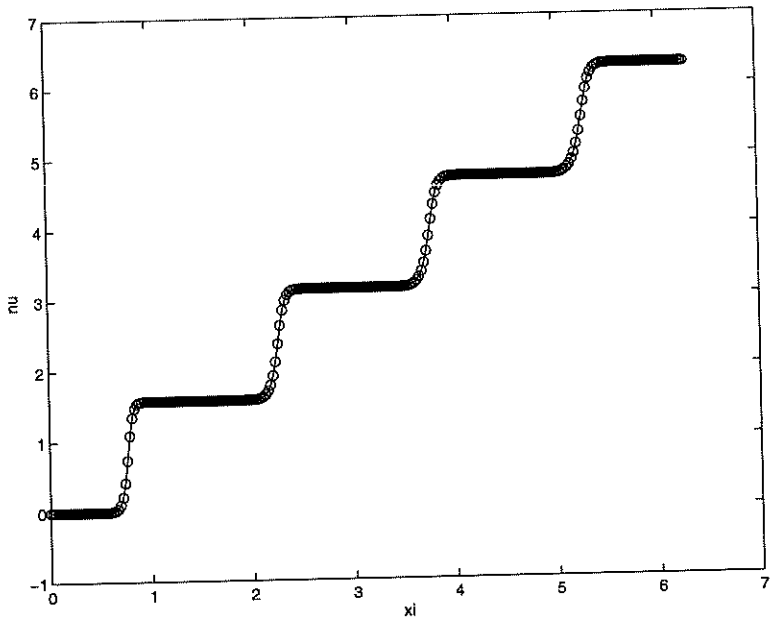

FIGURE 13. *Solution of the conservation law computed with the 3rd order ENO scheme. The computation is done on* $[0, 2\pi]$ *with* 256 *grid points to time* $t = 1.5$.

Example 3. (3D) We start from a sphere and evolve it with normal velocity equal to $\gamma(\nu, \varphi)$, where ν and φ are the spherical coordinates, $-\pi \le \nu \le \pi$, $-\frac{\pi}{2} \le \varphi \le \frac{\pi}{2}$. We use a grid of $100 \times 100 \times 100$. We choose $\gamma(\nu, \varphi) = \gamma(\nu) h_i(\varphi)$ for $i = 1, 2$ and 3. In figure 23, $h_1(\varphi) = 1 + 2|\sin(\varphi)|$, and the corresponding Wulff shapes are prisms with different bases that depend on $\gamma(\nu)$. In figure 24, $h_2(\varphi) = 1 + 2\sqrt{|\sin\frac{3}{2}(\varphi + \frac{\pi}{2})|}$, and the corresponding Wulff shapes are pyramids with different bases depending on $\gamma(\nu)$. $h_3(\varphi) = 1 + 2\sqrt{|\sin(|\varphi| - \frac{\pi}{6})|}$, and the corresponding Wulff shapes are bi-pyramids with various bases depending on $\gamma(\nu)$.

Example 4. We define

$$\gamma(\hat{n}) = 1 + 2\sqrt{|\max_{1 \le i \le 20} \hat{n} \cdot \mathbf{v}_i - 1|}$$

where the $\mathbf{v}_i$'s are the twenty vertices of a regular polygon of 12 faces that inscribes a unit sphere. We can expect that with the given surface intensity γ, the Wulff shape obtained from Wulff's geometric construction is a regular polygon of 12 faces, a soccer ball like object. We demonstrate this conjecture by starting with a sphere, growing it with the above defined γ. See figure 25 for the numerical result. We use a $100 \times 100 \times 100$ grid in our computation.

Example 5. In this example, we study the behavior of the ratio $E/V^{1-1/d}$ in the evolution process. Here $E = \int_\gamma \gamma(\hat{n}) dA$ is surface energy, V is the volume enclosed by the surface. In a recent paper [19] of Osher and Merriman, it was shown that, starting from a convex initial shape, this ratio decreases to its minimum as a shape grows outward normal to itself with velocity $\gamma(\nu)$, and the decreasing is strict unless the shape is the Wulff shape. This was proven for a general, not necessarily convex, γ. In the level set formulation,

$$\frac{E}{V^{1-1/d}} = \frac{\int \gamma(\frac{\nabla\phi}{|\nabla\phi|}) \delta(\phi) |\nabla\phi| dx}{\int H(-\phi) dx} \tag{8.10}$$

where $\delta(\phi)$ is the 1D δ function, $H(\phi)$ is 1D Heaviside function, d = 2 or 3 is the dimension.

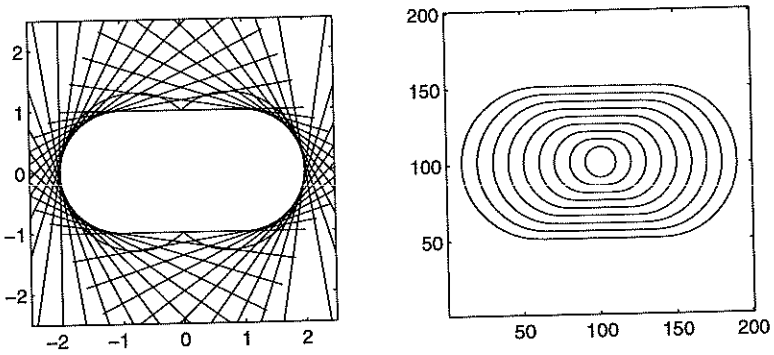

FIGURE 14. $\gamma(\nu) = 1 + |\sin(\nu + \frac{\pi}{2})|$.

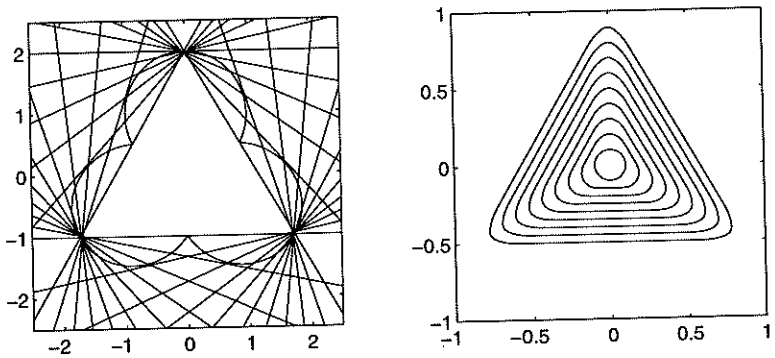

FIGURE 15. $\gamma(\nu) = 1 + |\sin(\frac{3}{2}(\nu + \frac{\pi}{2}))|$.

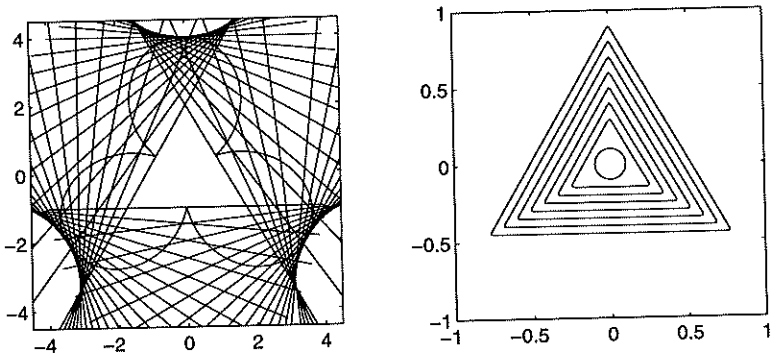

FIGURE 16. $\gamma(\nu) = 1 + 3|\sin(\frac{3}{2}(\nu + \frac{\pi}{2}))|$.

In our computation, $\delta(\phi)$ is approximated by:

$$\delta(\phi) = \begin{cases} 0 & \text{if } |\phi| \geq \epsilon, \\ -\frac{1}{6\epsilon}(1 + \cos(\frac{\pi x}{\epsilon})) & \text{if} |\phi| \geq \frac{\epsilon}{2}, \\ -\frac{1}{6\epsilon}(1 + \cos(\frac{\pi x}{\epsilon})) + \frac{4}{3\epsilon}(1 + \cos(\frac{2\pi x}{\epsilon})) & \text{otherwise.} \end{cases} \tag{8.11}$$

The Heaviside function $H(\phi)$ is approximated by:

$$H(\phi) = \begin{cases} 0 & \text{if } \phi \leq -\epsilon, \\ -\frac{1}{6}(1 + \frac{x}{\epsilon} + \frac{1}{\pi}\sin(\frac{\pi x}{\epsilon})) & \text{if } \phi \leq -\frac{\epsilon}{2}, \\ -\frac{1}{6}(1 + \frac{x}{\epsilon} + \frac{1}{\pi}\sin(\frac{\pi x}{\epsilon})) + \frac{1}{3}(2 + \frac{4x}{\epsilon} + \frac{1}{\pi}\sin(\frac{2\pi x}{\epsilon})) & \text{if } \phi \leq \frac{\epsilon}{2}, \\ -\frac{1}{6}(1 + \frac{x}{\epsilon} + \frac{1}{\pi}\sin(\frac{\pi x}{\epsilon})) + \frac{4}{3} & \text{if } x \leq \epsilon, \\ 1 & \text{otherwise.} \end{cases} \tag{8.12}$$

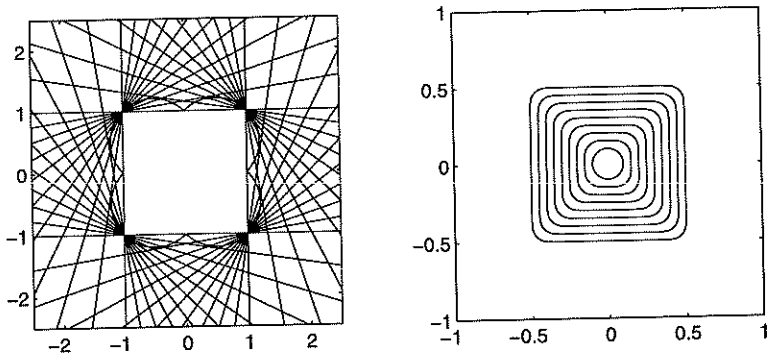

FIGURE 17. $\gamma(\nu) = |\cos(\nu)| + |\sin(\nu)|$.

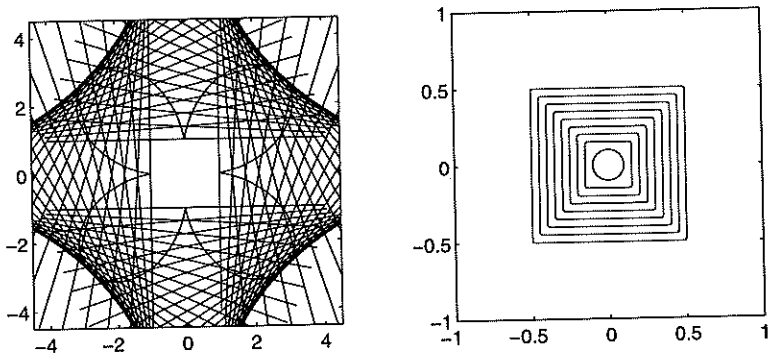

FIGURE 18. $\gamma(\nu) = 1 + 3|\sin(2\nu)|$.

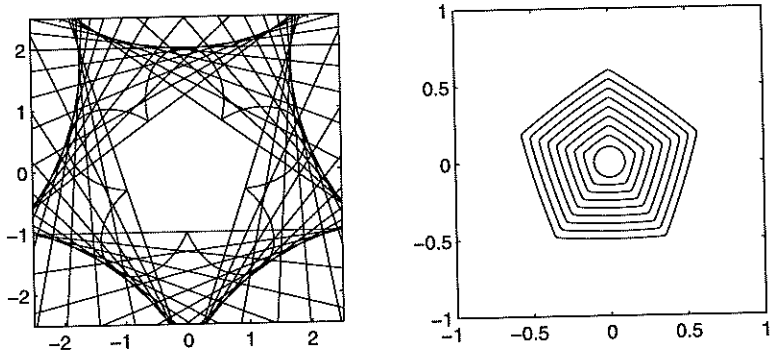

FIGURE 19. $\gamma(\nu) = 1 + |\sin(\frac{5}{2}(\nu + \frac{\pi}{2}))|$.

where $\epsilon = 3\Delta x$.

We start with a circle in 2D and a sphere in 3D. As was show in [19], the ratio decreases, and is a convex function of time. If we start from a nonconvex shape, our computations seem to show that this ratio also decreases.

Example 6. In this example, we start from a nonconvex, multiply connected shape and show how it grows, merges and finally asymptotes to a Wulff shape. This demonstrates the versatility and simplicity of our method. See figure 28 and 29.

9. Appendix

I. Proof of Lemma 2.2. In this appendix, we prove the following result stated in section 2.3.

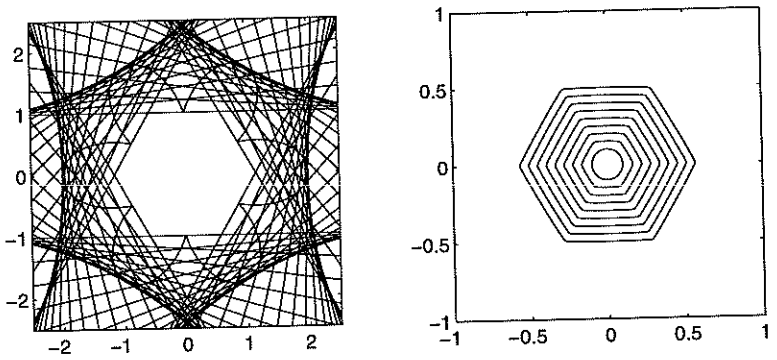

FIGURE 20. $\gamma(\nu) = 1 + |\sin(3(\nu + \frac{\pi}{2}))|$.

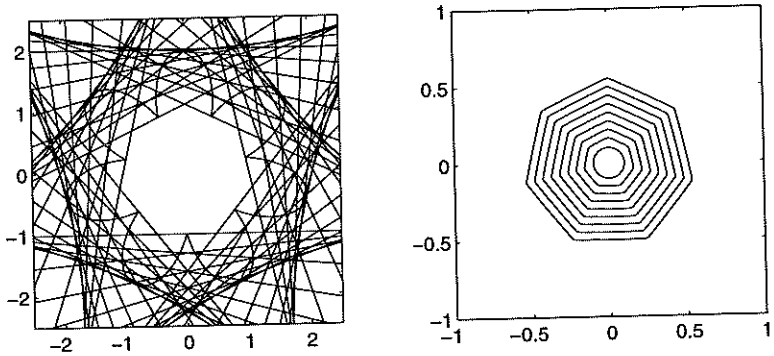

FIGURE 21. $\gamma(\nu) = 1 + |\sin(\frac{7}{2}(\nu + \frac{\pi}{2}))|$.

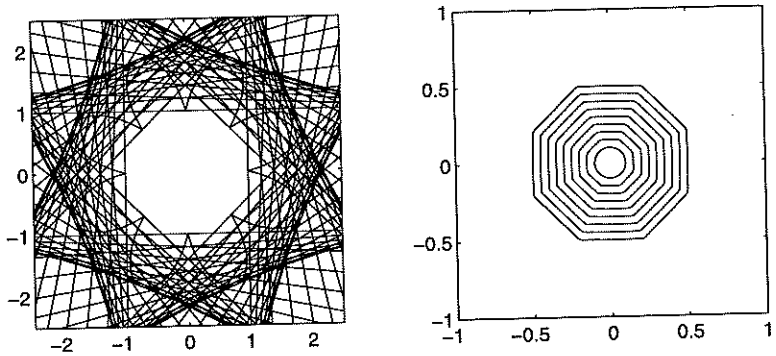

FIGURE 22. $\gamma(\nu) = 1 + |\sin(4\nu)|$.

Lemma 2.2 *γ is convex if and only if its homogeneous extension of degree 1 $\bar{\gamma} : R^d \to R^+$ is a convex function on R^d.*

Proof: Suppose the homogeneous extension of degree 1 $\bar{\gamma} : R^d \to R^+$ is a convex function on R^d. Hence the region $K = \{ x : \bar{\gamma}(x) \leq 1 \}$ is convex. But $K = \{ x : |x|\gamma(\frac{x}{|x|}) \leq 1 \} = \{ x : |x| \leq \frac{1}{\gamma(\frac{x}{|x|})} \}$ which is the region enclosed by the polar plot of $\frac{1}{\gamma}$. By definition, γ is convex.

On the other hand, suppose $\gamma : S^{d-1} \to R^+$ is convex, i.e. $K = \{ x : |x| \leq \gamma^{-1}(\frac{x}{|x|} \}$ is convex. Note $K = \{ x : |x|\gamma(\frac{x}{|x|}) \leq 1 \} = \{ x : \bar{\gamma}(x) \leq 1 \}$ since $\bar{\gamma}$ is a degree 1 homogeneous function. We further conclude that

$$K_c = \{ x : \bar{\gamma}(x) \leq c \}$$

is convex for any $c > 0$. We claim that this implies $\bar{\gamma}$ is convex over R^d.

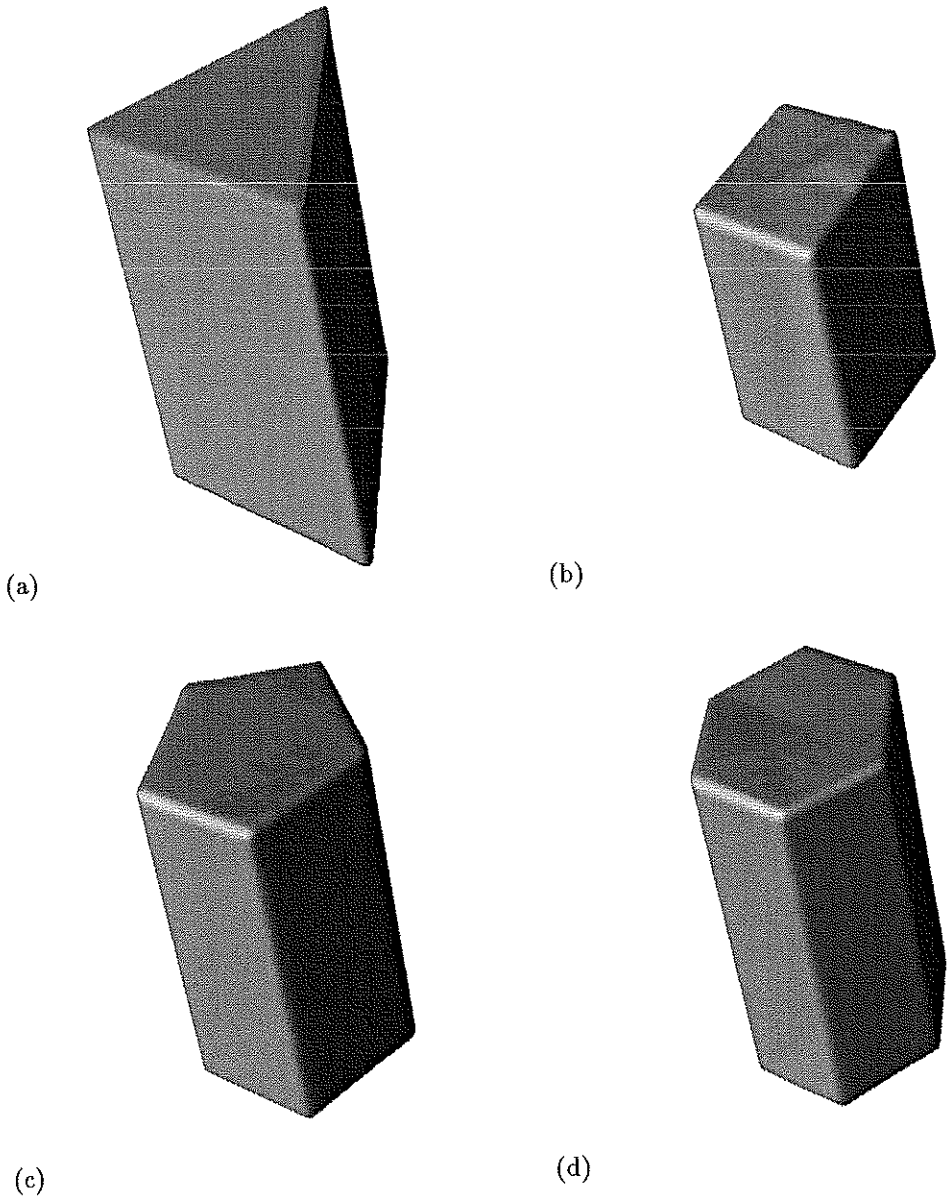

FIGURE 23. Wulff shape of prism. (a) $\gamma(\nu,\varphi) = (1+3|\sin(\frac{3}{2}(\nu+\frac{\pi}{2}))|)h_1(\varphi)$. (b) $\gamma(\nu,\varphi) = (1+|\sin(2(\nu+\frac{\pi}{2}))|)h_1(\varphi)$. (c) $\gamma(\nu,\varphi) = (1+|\sin(\frac{5}{2}(\nu+\frac{\pi}{2}))|)h_1(\varphi)$. (d) $\gamma(\nu,\varphi) = (1+|\sin(3(\nu+\frac{\pi}{2}))|)h_1(\varphi)$.

Refer to figure 30. Pick any two points P and Q from R^d, and a arbitrary $t \in (0,1)$. Without loss of generality, let us assume $\bar{\gamma}(P) < \bar{\gamma}(Q)$. Let Γ_0, Γ_t and Γ_1 be the level contour of $\bar{\gamma}$ taking values $\bar{\gamma}(P), (1-t)\bar{\gamma}(P) + t\bar{\gamma}(Q)$ and $\bar{\gamma}(Q)$, respectively. Let the origin of R^d be denoted as O, and the half line OP emanating from O intersect Γ_t at T and Γ_1 at R, and the line segment $\overline{OQ}$ intersect Γ_0 at S and Γ_t at U. Denote $\alpha = \frac{\bar{\gamma}(Q)}{\bar{\gamma}(P)}$. Then since $\bar{\gamma}$ is homogeneous function of degree 1, $R = \alpha P$ and $T = (1-t)P + tR$. Note that since $\frac{|P|}{|R|} = \frac{|S|}{|Q|}$, we have $PS \parallel RQ$. Similarly, $TU \parallel RQ$. Suppose $\overline{PQ}$ intersects $\overline{TU}$ at W, then $\frac{|PW|}{|PQ|} = \frac{|PT|}{|PR|} = t$. Hence $W = (1-t)P + tQ$. Since the region K_t enclosed by Γ_t is convex, we have $W \in K_t$ and therefore $\bar{\gamma}(W) \le \bar{\gamma}(T)$, which is $\bar{\gamma}((1-t)P + tQ) \le (1-t)\bar{\gamma}(P) + t\bar{\gamma}(Q)$.

II. The Evolution Equation for the Normal Angle in 2D. In this section, we derive the evolution equation which governs the motion of the normal angle of a growing shape in 2D. It is stated without proof

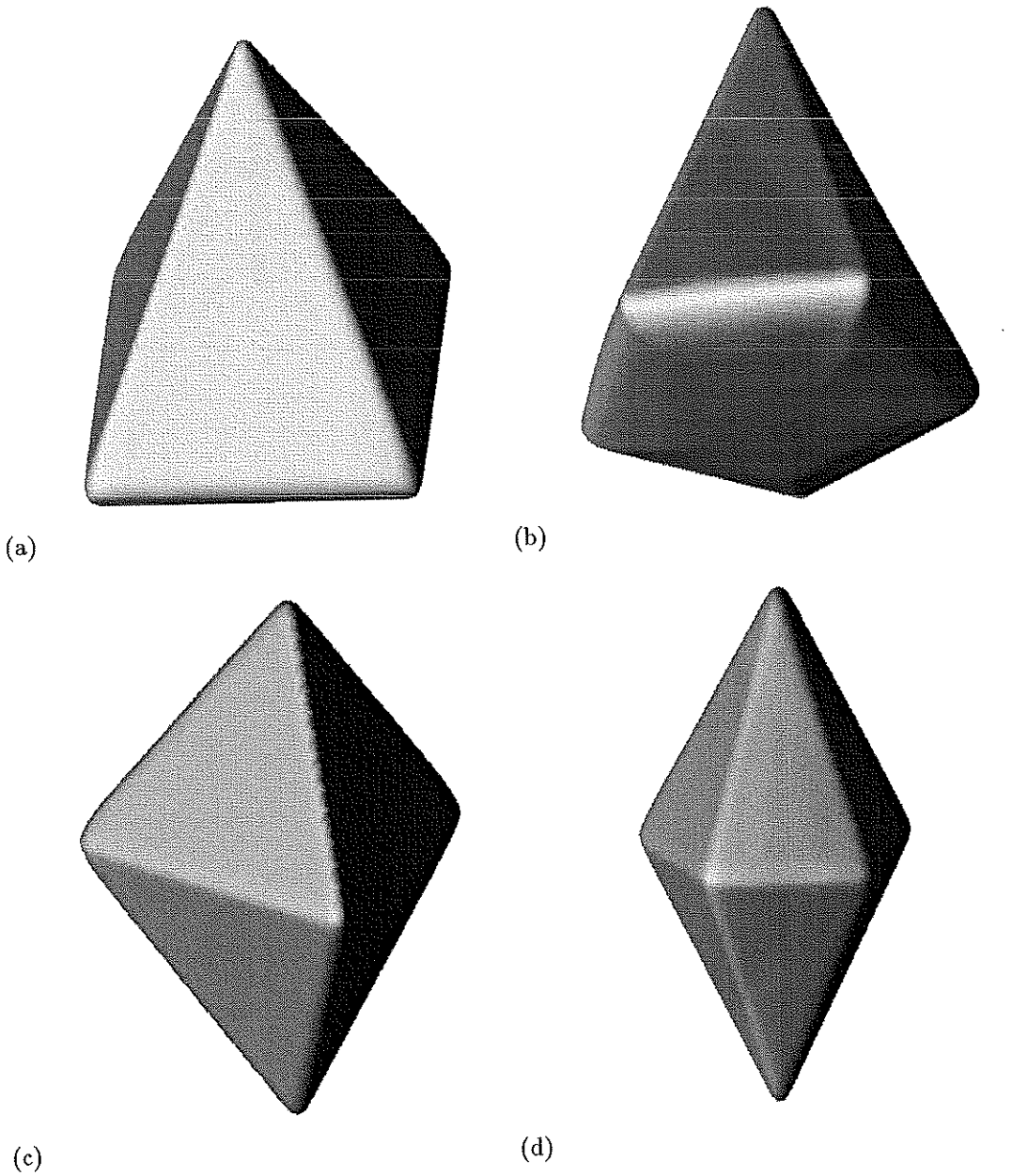

FIGURE 24. *Wulff shape of pyramid and bi-pyramid.* *(a)* $\gamma(\nu,\varphi) = (1+|\sin(2(\nu+\frac{\pi}{2}))|)h_2(\varphi)$. *(b)* $\gamma(\nu,\varphi) = (1+|\sin(\frac{5}{2}(\nu+\frac{\pi}{2}))|)h_2(\varphi)$. *(c)* $\gamma(\nu,\varphi) = (1+|\sin(\frac{3}{2}(\nu+\frac{\pi}{2}))|)h_3(\varphi)$. *(d)* $\gamma(\nu,\varphi) = (1+|\sin(\frac{5}{2}(\nu+\frac{\pi}{2}))|)h_3(\varphi)$.

in section 5.2 for the special case when the curve is a Wulff shape. A good reference on this topic is [12]. Let $\mathbf{r} : S^1 \to R^2$ be a smooth simple closed curve in 2D that is parameterized by α.

Let the curve move with normal velocity V, which may depend on some local or global properties of the curve. If we denote the curve at some later time t as $\mathbf{r}(t,\alpha)$, then

$$\frac{\partial \mathbf{r}}{\partial t} = V\hat{n}, \tag{9.1}$$

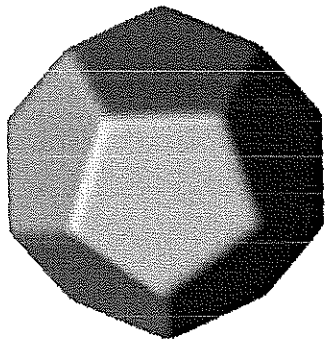

FIGURE 25. *A regular 12 polygon growed from a sphere with surface energy.*

where the partial derivative $\frac{\partial}{\partial t}$ is taken for α fixed. Similarly, the partial derivative $\frac{\partial}{\partial \alpha}$ is taken for t fixed. We want to make this point clear since some confusion may arise in the following analysis.

Let $w(t,\alpha) = |\frac{\partial \mathbf{r}}{\partial \alpha}(t,\alpha)|$ and s be the arclength parameter, which is only defined up to a constant. However $\frac{\partial}{\partial s}$ is well defined in the following sense

$$\frac{\partial}{\partial s} = \frac{1}{w(t,\alpha)}\frac{\partial}{\partial \alpha}. \tag{9.2}$$

Note that t and s may not be independent variables, and thus

$$\frac{\partial}{\partial t}\frac{\partial}{\partial s} \neq \frac{\partial}{\partial s}\frac{\partial}{\partial t}. \tag{9.3}$$

Let $\hat{\tau} = \frac{\partial \mathbf{r}}{\partial s}$ be the unit tangent vector, and $\hat{n}$ the unit outwards normal. Denote by θ the angle between $\mathbf{r}$ and the positive x-axis, and ν the angle between $\hat{n}$ and the positive x-axis. The Frechet formulae give us:

$$\begin{cases} \frac{\partial \hat{\tau}}{\partial \alpha} &= -w\kappa\hat{n}, \\ \frac{\partial \hat{n}}{\partial \alpha} &= w\kappa\hat{\tau}. \end{cases} \tag{9.4}$$

Using these relations, it is easy to show that:

$$\frac{\partial w}{\partial t} = \kappa V w \tag{9.5}$$

and

$$\frac{\partial}{\partial t}\frac{\partial}{\partial s} = \frac{\partial}{\partial s}\frac{\partial}{\partial t} - \kappa V\frac{\partial}{\partial s}. \tag{9.6}$$

For proofs of the above results and more details, please refer to [**12**].

Applying the above results to $\hat{n}$ and $\hat{\tau}$, we get

LEMMA 9.1.

$$\frac{\partial \hat{n}}{\partial t} = -\frac{\partial V}{\partial s}\hat{\tau}, \quad \frac{\partial \hat{\tau}}{\partial t} = \frac{\partial V}{\partial s}\hat{n}. \tag{9.7}$$

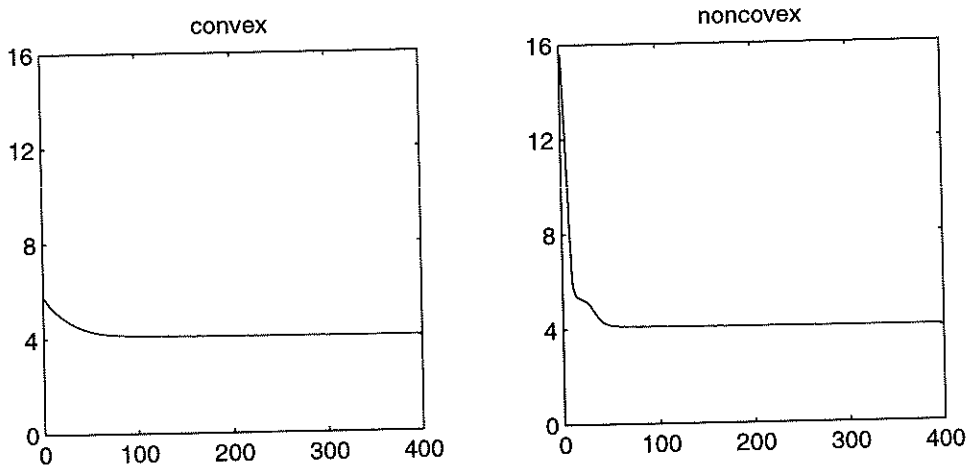

FIGURE 26. 2D.$\gamma(\nu) = |\cos(\nu)| + |\sin(\nu)|$.

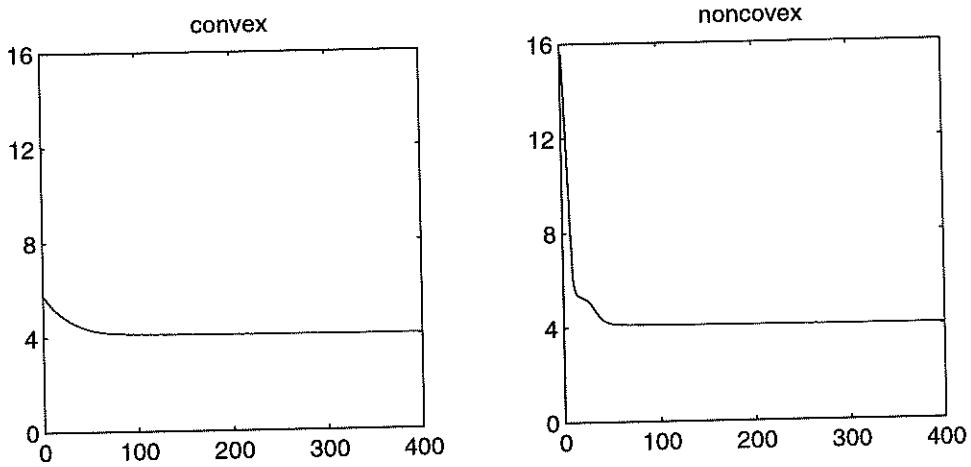

FIGURE 27. 3D.$\gamma(\hat{n}) = |n_x| + |n_y| + |n_z|$.

Proof:

$$\begin{aligned}
\frac{\partial \hat{\tau}}{\partial t} &= \frac{\partial}{\partial t}\frac{\partial \gamma}{\partial s} = \frac{\partial}{\partial s}\frac{\partial \gamma}{\partial t} - \kappa V \frac{\partial \gamma}{\partial s} \\
&= \frac{\partial}{\partial s}(V\hat{n}) - \kappa V \hat{\tau} = \frac{\partial V}{\partial s}\hat{n} \\
0 &= \frac{\partial}{\partial t} < \hat{n}, \hat{\tau} > = < \frac{\partial \hat{n}}{\partial t}, \hat{\tau} > + < \hat{n}, \frac{\partial \hat{\tau}}{\partial t} > \\
&= < \frac{\partial \hat{n}}{\partial t}, \hat{\tau} > + \frac{\partial V}{\partial s}.
\end{aligned}$$

□

Hence the first equality.

From the above Lemma, we immediately get:

$$\frac{\partial \nu}{\partial t} = -\frac{\partial V}{\partial s}. \tag{9.8}$$

Now we introduce the time/arclength coordinate system:

$$\begin{cases} \tau = t \\ s = s(t,\alpha) = \int_0^\alpha w(t,\alpha)d\alpha \end{cases} \tag{9.9}$$

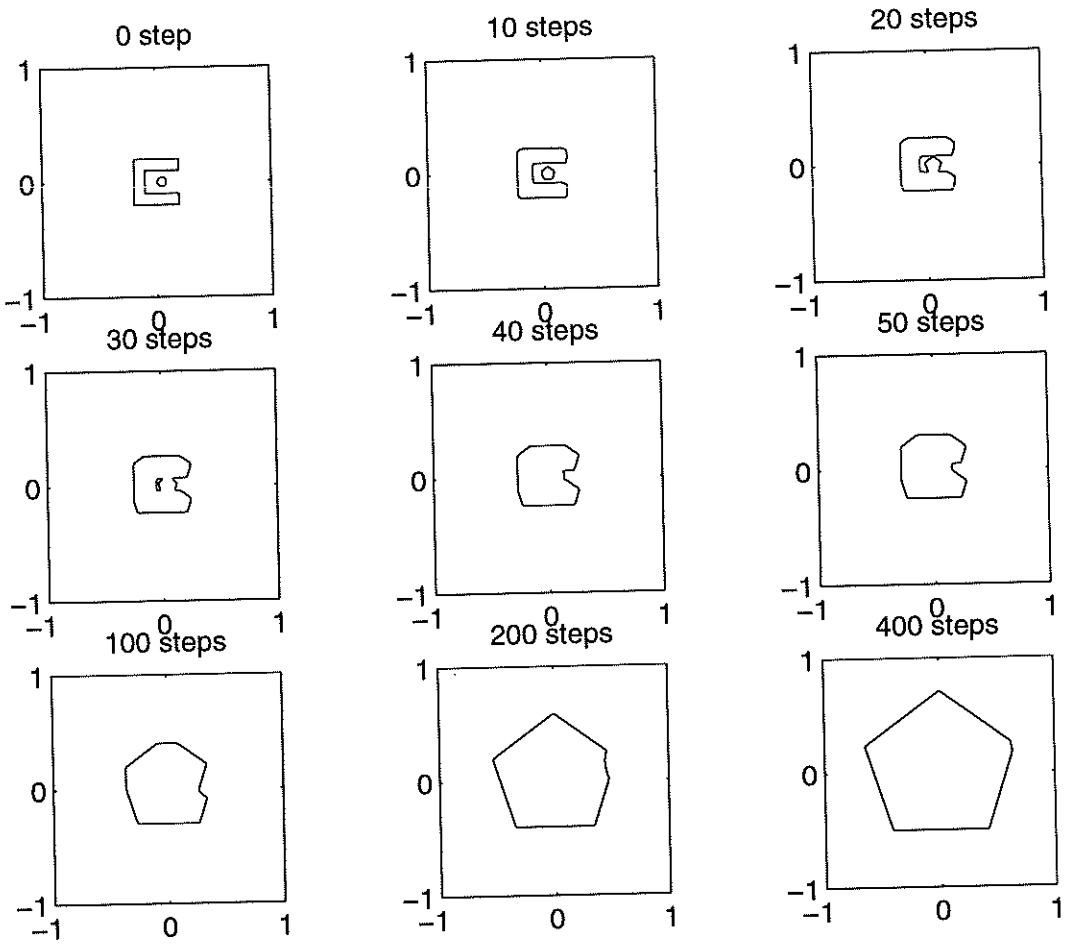

FIGURE 28. *The growing and merging of the initial nonconvex and multiply connected shape into the Wulff shape.* $\gamma(\nu) = 1 + |\sin(\frac{5}{2}(\nu + \frac{\pi}{2})|$.

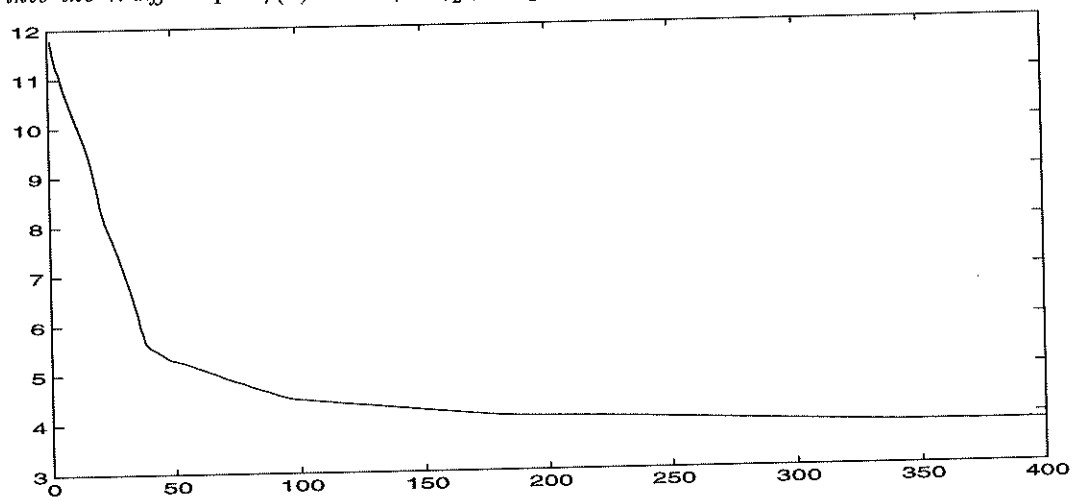

FIGURE 29. *The change of energy and area ratio in the above process.*

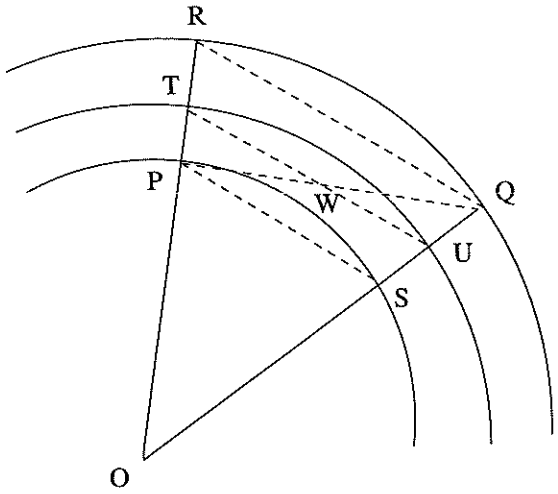

FIGURE 30. Contour of a homogeneous function of degree 1.

In the this system, we have

$$\begin{aligned}\frac{\partial \nu}{\partial t} &= \frac{\partial \nu}{\partial \tau} + \frac{\partial \nu}{\partial s}\frac{\partial s}{\partial t},\\ \frac{\partial s}{\partial t} &= \int_0^\alpha \frac{\partial w}{\partial t} d\alpha = \int_0^\alpha \kappa V w d\alpha\\ &= \int_0^s V\kappa ds = \int_{\nu_0}^\nu V d\nu,\end{aligned}$$

where ν_0 is the normal angle of the reference point with $\alpha = 0$. Note that

$$\frac{\partial V}{\partial s} = \frac{\partial V}{\partial \nu}\frac{\partial \nu}{\partial s}.$$

We thus obtain the evolution equation for ν in this system:

$$\frac{\partial \nu}{\partial \tau} + \left[\int_{\nu_0}^\nu V(\nu) d\nu + \frac{\partial V}{\partial \nu}\right]\frac{\partial \nu}{\partial s} = 0. \tag{9.10}$$

In the self-similar growth of Wulff crystals, the velocity $V = \gamma(\nu)$ and we can choose the reference point so that $\nu_0 \equiv 0$ and $\gamma'(0) = 0$. We replace τ by t and get

$$\frac{\partial \nu}{\partial t} + \int_0^\nu [\gamma(u) + \gamma''(u)]\, du \frac{\partial \nu}{\partial s} = 0. \tag{9.11}$$

This conservation law gives incorrect jump conditions at corners. The correct equation can be obtained by a change of variables in the equation (9.11) that governing the evolution of normal angle. We introduce the following new set of variables:

$$\begin{cases} \tau = t, \\ \xi = t\theta(t,s) \end{cases} \tag{9.12}$$

where $\theta(t,s)$ is defined implicitly by:

$$\frac{s}{t} = \int_0^\theta \sqrt{W^2(\theta) + W'^2(\theta)}\, d\theta = \int_0^{\nu(\theta)} [\gamma(\nu) + \gamma''(\nu)]\, d\nu \tag{9.13}$$

and $\nu(\theta)$ in turn is defined by

$$\theta = \nu + \tan^{-1}\left(\frac{\gamma'(\nu)}{\gamma(\nu)}\right),$$

where $W(\theta) = \gamma_*(\theta)$.

By the chain rule, we have

$$\begin{aligned}\frac{\partial \nu}{\partial t} &= \frac{\partial \nu}{\partial \tau} + \frac{\partial \nu}{\partial \xi}\frac{\partial \xi}{\partial t},\\ \frac{\partial \nu}{\partial s} &= \frac{\partial \nu}{\partial \xi}\frac{\partial \xi}{\partial s},\\ \frac{\partial \xi}{\partial t} &= \theta + t\frac{\partial \theta}{\partial t},\\ \frac{\partial \xi}{\partial s} &= t\frac{\partial \theta}{\partial s}.\end{aligned}$$

We have the following

$$\begin{aligned}\frac{\partial \theta}{\partial t} &= -\frac{s}{t^2}\frac{\gamma(\nu)}{\gamma^2(\nu)+\gamma'^2(\nu)},\\ \frac{\partial \theta}{\partial s} &= \frac{1}{t}\frac{\gamma(\nu)}{\gamma^2(\nu)+\gamma'^2(\nu)}\end{aligned}$$

and thus

$$\begin{aligned}\frac{\partial \nu}{\partial t} &= \frac{\partial \nu}{\partial \tau} + \frac{\partial \nu}{\partial \xi}\left(\theta - \frac{s}{t}\frac{\gamma(\nu)}{\gamma^2(\nu)+\gamma'^2(\nu)}\right),\\ \frac{\partial \nu}{\partial s} &= \frac{\partial \nu}{\partial \xi}\frac{\gamma(\nu)}{\gamma^2(\nu)+\gamma'^2(\nu)}.\end{aligned}$$

Inserting these expression into equation (9.11), we get

$$\frac{\partial \nu}{\partial \tau} + \frac{\partial F(\nu)}{\partial \xi} = 0,$$

where $F(\nu) = \frac{\nu^2}{2} + \int_0^\nu \tan^{-1}\frac{\gamma'(u)}{\gamma(u)}du$.

III. The Euler-Lagrange Equation of Surface Energy. The Lagrangian (7.3) when γ is a homogeneous function of degree 1 is of the following form

$$\mathcal{L}(\phi,\lambda) = \int \gamma(\nabla\phi)\delta(\phi)|\nabla\phi|dx - \lambda\int H(-\phi)dx. \tag{9.14}$$

Take $\psi \in C_0^\infty$, we have

$$\begin{aligned}<\frac{\delta\mathcal{L}}{\delta\phi},\psi> &\stackrel{def}{=} \lim_{\epsilon\to 0}\frac{1}{\epsilon}[\mathcal{L}(\phi+\epsilon\psi,\lambda)-\mathcal{L}(\phi,\lambda)]\\ &= \int\{D\gamma(\nabla\phi)\cdot\nabla\psi\delta(\phi)+\gamma(\nabla\phi)\delta\prime(\phi)\psi+\delta(-\phi)\psi\}dx\\ &= \int\{-\nabla\cdot[\delta(\phi)D\gamma(\nabla)]+\gamma(\nabla\phi)\delta\prime(\phi)+\lambda\delta(\phi)\}\psi dx\\ &= \int\{-\delta\prime(\phi)\nabla\cdot D\gamma(\nabla\phi)-\delta(\phi)\nabla\cdot D\gamma(\nabla)+\gamma(\nabla\phi)\delta\prime(\phi)-\lambda\delta(\phi)\}\\ &= -\int\{\nabla\cdot D\gamma(\nabla\phi)-\lambda\}\delta(\phi)\psi dx\\ &= -\int\{\nabla\cdot D\gamma(\nabla\phi)-\lambda\}\frac{\psi}{|\nabla\phi|}\delta(\phi)|\nabla\phi|dx.\end{aligned}$$

Hence the Euler-Lagrange equation is

$$\nabla\cdot D\gamma(\nabla\phi) = \lambda, \tag{9.15}$$

where the Lagrange constant λ is chosen such that the volume enclosed is as given.

Noting that when γ is a homogeneous function of degree 1, then $D\gamma$ is homogeneous of degree 0 and hence $\gamma(\nabla\phi) = \gamma(\frac{\nabla\phi}{|\nabla\phi|})$.

For extensions of γ which are not necessarily homogeneous of degree 1, the Euler-Lagrange equation can be obtained through a similar but more involved calculation and is found to be

$$\nabla \cdot [\gamma(\hat{n}) + \nabla_{\hat{n}}\gamma(\hat{n}) - (\nabla_{\hat{n}}\gamma(\hat{n}) \cdot \hat{n})\hat{n}] = 0. \tag{9.16}$$

where $\hat{n} = \frac{\nabla\phi}{|\nabla\phi|}$ is function of space variable x, and the ∇ means gradient with respect to x, and $\nabla_{\hat{n}}$ means gradient with respect to the variables of (extended) γ.

For example, if we extend γ to be constant in the radial direction, then $\nabla_{\hat{n}}\gamma(\hat{n}) \cdot \hat{n} = 0$ and the Euler-Lagrange equation would be

$$\nabla \cdot [\gamma(\hat{n}) + \nabla_{\hat{n}}\gamma(\hat{n})] = 0, \tag{9.17}$$

which is different from equation (9.15). We will use the homogeneous extension of degree 1 next.

The gradient flow of the surface energy with the volume constraints is

$$\phi_t = |\nabla\phi| \left[\nabla D\gamma \left(\frac{\nabla\phi}{|\nabla\phi|} \right) - \lambda \right],$$

where

$$\lambda = \frac{\int \nabla \cdot \left[D\gamma(\frac{\nabla\phi}{|\nabla\phi|}) \right] \delta(\phi)|\nabla\phi| dx}{\int \delta(\phi)|\nabla\phi| dx}. \tag{9.18}$$

The reason that we have included the extra term $|\nabla\phi|$ is to make the above equation rescaling invariant, i.e. ϕ can be replaced by $h(\phi)$ with $h' > 0$ and $h(0) = 0$.

The surface energy on the gradient flow is diminishing. To see this, let

$$\mathcal{F} = \nabla \cdot D\gamma(\nabla\phi)$$

and we have

$$\begin{aligned} \frac{dE}{dt} &= \frac{d}{dt} \int \gamma(\nabla\phi)\delta(phi)dx \\ &= -\int \mathcal{F}(\mathcal{F} - \lambda)\delta(phi)|\nabla\phi|dx \\ &= -\int_{\gamma} \mathcal{F}(\mathcal{F} - \lambda)dA. \end{aligned}$$

where $dA = \delta(\phi)|\nabla\phi|dx$ is area element in 3D and arclength element in 2D. Using the Schwarz inequality

$$|\int_{\gamma} \mathcal{F} dA|^2 \leq \int_{\gamma} \mathcal{F}^2 dA \int_{\gamma} dA, \tag{9.19}$$

one easily sees that

$$\frac{dE}{dt} \leq 0. \tag{9.20}$$

References

[1] D. Adalsteinsson and J. A. Sethian, *A Fast Level Set Method for Propagating Interfaces*, J. Comput. Phys., v118, pp. 269-277, 1995

[2] J. E. Brothers and F. Morgan, *The Isoperimetric Theorem for General Integrands*, Michigan Math. J., 41 (1994), no. 3, pp. 419-431.

[3] J.W. Cahn, J. E. Taylor, and C. A. Handwerker, *Evolving Crystal Forms: Frank's Characteristics Revisited*, a chapter in Sir Charles Frank, OBE, FRS: An Eightieth Birthday Tribute, eds. R. G. Chambers, J. E. Enderby, A. Keller, A. R. Lang and J.W. Steeds, published by Adam Hilger Co., Bristol, England, 1991.

[4] A.A. Chernov, *The Kinetics of the Growth Form of Crystals*, Soviet Physics Crystallography, v7 (1963), pp.728-730, translated from Krystallografiya, v7 (1962) pp. 895-898.

[5] A.A. Chernov, *Modern Crystallography III, Crystall Growth*, Springer-Verlag, Berlin (1984).

[6] R. Courant and K.-O. Friedrichs, Supersonic Flow and Shock Waves, Wiley, Interscience, 1962.

[7] R. Caflisch, M. Gyure, B. Merriman, S. Osher, C. Ratsch, D. Vredensky and J. Zinck, *Island Dynamics and the Level Set Method for Epitaxial Growth*, Applied Math. Letters, 1999, to appear.

[8] M.G. Crandall and P.L. Lions, *Two approximations of solutions of Hamilton-Jacobi equations*, Math. Comput., v43, 1984, pp. 1-19.

[9] I. Fonseca, *The Wulff Theorem Revisited*, Proc. Royal Soc. London A, v432 (1991) pp. 125-145

[10] F.C. Frank, *The Geometrical Thermodynamics of Surfaces, in Metal Surfaces: Structure, Energies and Kinetics*, Am. Soc. Metals, Metals Park, Ohio, 1963.
[11] M. E. Gurtin, Thermomechanics of Evolving Phase Boundaries in the Plane, Clarendon Press, Oxford, 1993.
[12] M. Gage and R. S. Hamilton, *The Heat Equation Shrinking Convex Plane Curves*, J. Differental Geometry, 23(1986) 69-96.
[13] C. Herring, chapter in *The Physics of Powder Metallurgy*, edited by W. E. Kingston, McGraw-Hill Book Co., New York, 1951.
[14] G. S. Jiang and D. Peng, *WENO Schemes for Hamilton-Jacobi equations*, UCLA CAM report 97-29, 1997. To appear in SIAM J. Sci. Comput.
[15] S. Osher, *The Riemann Problem for Nonconvex Scalar Conservation Laws and Hamilton-Jacobi Equations*, Proc. Amer. Math. Soc., v 89, pp 641-645, 1983.
[16] S. Osher, *Riemann Solvers, the Entropy Condition and Difference Approximation.* SIAM J. Numer. Anal. 21(1984) pp217-235.
[17] S. Osher and J. Sethian, *Fronts propagating with curvature dependent speed: algorithms based on Hamilton-Jacobi formulations*, J. Comput. Phys., v79, 1988, pp. 12-49.
[18] S. Osher and C-W. Shu, *High-order essentially non-oscillatory schemes for Hamilton-Jacobi equations*, J. Numer. Anal., v28, 1991, pp. 907-922.
[19] S. Osher and B. Merriman, *The Wulff Shape as the Asymptotic Limit of a Growing Crytalline Interface.* Asian J. Math., v1, no. 3, pp560-571, Sept. 1997.
[20] D. Peng, B. Merriman, S. Osher, H-K Zhao and M. Kang *A PDE Based Fast Local Level Set Method.* UCLA CAM Report 98-25. Submitted to J. Comp. Phys.
[21] B. Riemann, *Über die Forteflanzung ebener Luftwellen von enolicher Schwingungsweite, Abhandlungen der Gessellschaft der Wissenschafter zu Göttingen*, Mathematish-Physikalische Klasse 8, v. 43, 1860.
[22] S. Ruuth and B. Merriman, *Convolution Generated Motion and Generalized Huygens' Principles for Interface Motion.* UCLA CAM Report 98-4.
[23] C-W. Shu, *Total-Variation-Diminishing Time Discretization*, SIAM J. Sci. Stat. Comput. v9, pp. 1073-1084, 1988.
[24] C-W. Shu and S. Osher, *Efficient implementation of essentially non-oscillatory shock-capturing schemes II*, J. Comput. Phys., v83, 1989, pp. 32-78.
[25] J. A. Sethian, *A Fast Marching Level Set Method for Monotonically Advancing Fronts* Proc. Nat. Acad. Sci., v93, 4, pp. 1591-1595, 1996.
[26] M. Sussman, P. Smereka and S. Osher, *A Level Set Approach for Computing Solutions to Incompressible Two-Phase Flow*, vol. 114, no. 1, Sept. 1994, pp. 146-159.
[27] J. E. Taylor, *Existence and Structure of Solutions to a Class of Non-elliptic Variational Problems.* Symposia Mathematica v 14, pp 499-508, 1974.
[28] G. Wulff, *Zur Frage der Geschwindigkeit des Wachsthums und der Auflösung der Krystallflachen*, Zeitschrift für Krystallographie und Minerologie, v 34, pp 449-530, 1901.

Department of Mathematics, University of California, Los Angeles, CA 90095-1555
E-mail address: dpeng@math.ucla.edu

Department of Mathematics, University of California, Los Angeles, CA 90095-1555
E-mail address: sjo@math.ucla.edu

Department of Mathematics, University of California, Los Angeles, CA 90095-1555
E-mail address: barry@math.ucla.edu

Department of Mathematics, University of California, Los Angeles, CA 90095-1555
Current address: Department of Mathematics, Stanford University, Stanford, CA 74305-2125.
E-mail address: zhao@math.stanford.edu